

Investigation of porous materials with large surface heterogeneity using the generalized Porod's scattering law method

Wei-Shan Chiang,^{1,2} Jin-Hong Chen,³ and Yun Liu^{1,2,4,*}

¹*Center for Neutron Research, National Institute of Standards and Technology, Gaithersburg, Maryland 20899, USA*

²*Department of Chemical and Biomolecular Engineering, University of Delaware, Newark, Delaware 19716, USA*

³*Aramco Services Company: Aramco Research Center-Houston, Houston, Texas 77084, USA*

⁴*Department of Physics and Astronomy, University of Delaware, Newark, Delaware 19716, USA*



(Received 1 May 2018; published 9 April 2019)

Surface heterogeneity is ubiquitous in both natural and man-made materials, and can significantly influence material properties. However, it is very challenging to noninvasively probe the variation of surface properties in porous materials. Recently, we have proposed a method, i.e., the generalized Porod's scattering law method (GPSLM), to obtain the surface heterogeneity information in bulk porous materials by extending the classic Porod's scattering method. However, it was not clear if the GPSLM can be applied to other more complex materials, such as porous materials with dead pores, i.e., pores that guest fluid molecules cannot access or porous materials whose solid matrix can adsorb small guest molecules. In this paper, we theoretically extend the GPSLM to study those more complex situations. For all five cases with different levels of complexity discussed in this work, the scattering intensity at the Porod's law region always follows a parabolic function of scattering length density (SLD) of the guest fluid. Moreover, the minimum value of the scattering intensity is all related to the surface heterogeneity of the porous materials. The SLD of the guest fluid at which the minimum intensity is reached is always related to the surface-averaged SLD of materials. We also discuss the potential limitations and possible future applications of the GPSLM. As the GPSLM is based on the contrast variation method commonly used for a wide range of materials, such as geological materials, biomaterials, and colloidal suspensions, the theoretical development here is potentially useful for researchers who would like to apply the GPSLM to more complicated materials besides porous materials.

DOI: [10.1103/PhysRevE.99.042801](https://doi.org/10.1103/PhysRevE.99.042801)

I. INTRODUCTION

Surface heterogeneity represents the coexistence of different chemical and structural properties at the interfaces of a system and it is ubiquitous in both natural and industrial materials. Many studies have shown that the surface heterogeneity can greatly influence the interactions [1–4], mechanical properties [5,6], surface reaction rate [7], and transport phenomena [8–10]. It is therefore important to study the surface heterogeneity and further tune the surface properties of the materials to achieve desired properties in various fields such as the pharmaceutical industry [11–13], catalysis [14,15], microfluids [9,10], and petroleum engineering [8].

There are many methods commonly used for characterizing the surface heterogeneity of materials, including atomic force microscopy (AFM) [16], scanning electron microscopy (SEM) [5,6,17], energy dispersive spectroscopy (EDS) [5,6], x-ray photoelectron spectroscopy (XPS) [16], auger electron spectroscopy (AES) [18,19], and secondary ion mass spectrometry (SIMS) [20]. However, despite that these techniques are useful for many applications, they often require special sample preprocessing. There are always concerns that the

surface properties of the original materials may be altered during the material processing required by these techniques. Further, it is very challenging to apply these methods noninvasively to obtain the properties of the interfaces buried deeply inside porous materials [17,18]. There is therefore a strong need to develop noninvasive characterization methods to determine the surface heterogeneity.

Scattering techniques are good candidates for the nondestructive surface characterization. The well-known Porod's scattering law developed for analyzing x-ray or neutron scattering data [21,22] has been widely used to determine the surface area and the scattering length density (SLD) of materials in various two-phase systems such as biological macromolecules [23], colloids [24], and porous materials [25]. SLD is an intrinsic property of a material that only depends on molecular formula and density of the components in the materials. Despite its wide applications, the conventional Porod's scattering law, originally developed for a relatively homogeneous matrix, becomes less accurate when applied to heterogeneous systems such as natural rocks, cement pastes, and multiphase alloys because these systems have more than two phases. Moreover, the classic Porod's scattering can only report the average SLD of a material and total surface area. It cannot provide the information of the variation of the surface properties. This greatly limits the structure information that can be obtained from the scattering data of the heterogeneous samples.

*Corresponding author: yunliu@nist.gov; yunliu@udel.edu

In order to determine the surface heterogeneity, we have recently developed a surface characterization method, the generalized Porod's scattering law method (GPSLM) [26]. GPSLM is based on the conventional Porod's scattering law and the contrast variation method, both of which are already widely used in the scattering community. Some attempts have already been made to use contrast variation to determine the structure of heterogeneous natural materials such as shale rocks and coals [27,28]. However, these works still adopted the two-phase assumption and therefore much of the heterogeneity information was lost.

We previously demonstrated that the GPSLM [26] was very useful for porous materials that satisfy the following conditions: (1) there is a clear Porod's scattering law region in the isotropic scattering pattern, (2) all pores are accessible to the guest fluids used for the contrast variation, (3) the SLD of the solid matrix does not change when changing the SLD of the guest fluids inside pores. This method was successfully applied to study kerogen, a porous organic matter that is important for the gas and oil storage in shales. The average SLD of kerogens isolated from natural shale rocks was found to increase with the maturity of kerogens, indicating the decrease in hydrogen atom content with maturity. It was demonstrated theoretically that the average SLD of materials obtained by the GPSLM is a surface-averaged SLD, not volume-averaged SLD. It is further found that isolated kerogens can have large surface heterogeneity depending on their maturity. For the three studied kerogens, the less mature sample has a large variation of the SLD, implying a large variation of hydrogen content in the kerogen, while the more mature sample tends to have more uniform matrix.

However, many materials may have dead pores inside, i.e., not all pores can be accessed to guest molecules [27]. In addition, the solid matrix of some porous materials may change SLD during the contrast variation due to the adsorption of guest fluid molecules in "tiny" pores on the walls of pores. It thus remains an unanswered question of whether the GPSLM is applicable to these more complicated porous materials.

In this paper, we develop the theoretical framework to extend the GPSLM to more complicated situations. We focus on five different cases of porous materials with increasing level of complexity. Our previous work demonstrated the applicability of the GPSLM for the first case, the simplest case. We show in this work that for four other types of heterogeneous porous materials, the GPSLM is still applicable but the parameters have different meanings depending on the situations. We also discuss in detail the limitations of our method. Our method is useful to study more complicated porous materials such as shale rocks with imbedded kerogens.

The structure of this paper is organized as follows. In Sec. II, we introduce the theoretical background of the GPSLM and the general formulas used in the GPSLM. We also describe the five different types of porous materials studied in this paper, from the simplest one, case 1, to the most complicated and general one, case 5. Note that this classification is based on the assumptions used for the GPSLM method. Therefore, this classification is different from other classifications of porous materials based on different techniques, such as the gas isotherm type, according to the IUPAC Classification Scheme [29]. Sections II A, II B, II C, II D, and II E give

the mathematical expressions and physical meanings of the parameters in the general formulae of the GPSLM for case 1, case 2, case 3, case 4, and case 5, respectively. In Sec. III, a model system of case 2 is simulated and used as an example to demonstrate the validity and the data analysis procedure of the GPSLM. In Sec. IV, we discuss some limitations and possible solutions of the GPSLM. In Sec. V, we summarize the method of the GPSLM and explain some advantages of using GPSLM as a characterization method for the surface heterogeneity. Some potential systems that the GPSLM can apply to are also proposed. In Appendices A, B, C, D, and E, the derivations of the GPSLM formulas are provided for case 1, case 2, case 3, case 4, and case 5, respectively. Appendix F elaborates on the details of calculating the scattering intensity of the simulated system described in Sec. III. Appendix G gives the derivation of equations used in the potential remedy described in Sec. IV for the systems in which Porod's scattering region is not present explicitly but can be decoupled from other scattering features.

II. GENERALIZED POROD'S SCATTERING LAW METHOD (GPSLM)

The conventional Porod's scattering law [21,22] states that for two-phase systems with smooth interfaces, the coherent scattering intensity, $I(Q)$, at high Q can be asymptotically formulated as

$$I(Q) \xrightarrow{Q \rightarrow \infty} 2\pi \frac{S_T}{V} (\Delta\rho)^2 Q^{-4}, \quad (1)$$

where Q is the scattering wave vector, and the contrast term, $\Delta\rho = \rho_1 - \rho_2$, is the difference of the SLD between phase 1 and phase 2 in a two-phase system. S_T and V are the total surface area and total volume in a porous material, respectively, detected by the neutron or x-ray beam. The Porod's law scattering pattern, i.e., the scattering pattern with $I(Q) \propto Q^{-4}$, has been commonly seen in the scattering data obtained from small-angle neutron scattering (SANS) or small-angle x-ray scattering (SAXS) for many complicated systems [23,30,31]. In principle, the conventional Porod's law is only applicable to homogeneous two-phase systems [see Fig. 1(a)] or two-phase systems with small heterogeneity of the surface matrix. If the pore is empty, i.e., $\rho_2 = 0$, then $I(Q) \xrightarrow{Q \rightarrow \infty} 2\pi \frac{S_T}{V} (\rho_1)^2 Q^{-4}$. Thus, by using the Porod's scattering law, the SLD of the matrix, ρ_1 , or the total surface area, S_T , can be obtained.

However, for many porous materials, the SLD at different interfaces may have different values. To overcome the challenge to obtain the variation of the SLD of different surfaces, the GPSLM was recently developed [26] and shows that for some simple porous materials with smooth interfaces (case 1 porous material that will be defined later), the surface variation of SLD can be quantitatively obtained using scattering methods. Furthermore, it can provide a way to estimate the potential errors introduced by the conventional Porod's law using Eq. (1) that is mainly applicable to homogeneous systems.

In this paper, we extend the GPSLM [26] developed previously and demonstrate that the GPSLM is a powerful tool applicable to a wide range of materials, and provides additional material information that cannot be obtained using Eq. (1).

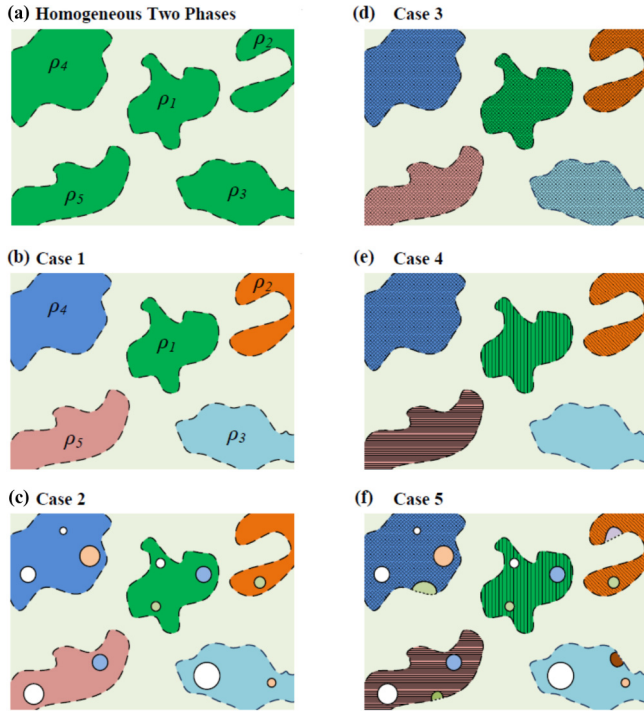


FIG. 1. (a) A homogeneous two-phase system. (b)–(f) Five different heterogeneous systems discussed in this work. The detectable structure is comparable to length scale of Porod’s Q range $\approx \frac{2\pi}{Q}$. (b) Case 1: solid matrix is not changed by loading fluid and all the pores with length scale $\approx L$ are accessible. (c) Case 2: solid matrix is not changed by loading fluid and there are inaccessible pores or compact solid pockets with length scale $\approx L$. (d) Case 3: solid domains have the same dependence of average domain SLD on guest fluid SLD and all the pores with length scale $\approx L$ are accessible. (e) Case 4: solid domains have different dependence of average domain SLD on guest fluid SLD and all the pores with length scale $\approx L$ are accessible. (f) Case 5: solid domains have different dependence of average domain SLD on guest fluid SLD and there are inaccessible pores or compact solid pockets with length scale $\approx L$. The solid lines outline the interfaces between the matrix and the pores or solid pockets inaccessible to the guest fluid; the dashed lines outline the interfaces between the matrix and the accessible open pores; the dotted lines [in (f)] outline the interfaces between inaccessible solid pocket (with nonchanging SLD) and open pores.

The GPSLM is also essential to provide a way to interpret the data for the contrast variation method at the Porod’s scattering region for heterogeneous samples. It should be noted that although the Porod’s scattering pattern can also be present in the scattering curves of anisotropic scatterers with smooth interfaces [32], the anisotropic effect should be considered carefully in the mathematical formula of the Porod’s constant. For anisotropic scatters with smooth interfaces, the Porod’s law is applicable if all scatters can be considered randomly oriented.

We will first show the general method of the GPSLM and briefly describe its experimental procedure. Then we will show the detailed meaning of the obtained results for the different types of porous materials.

GPSLM requires the use of contrast variation. To do contrast variation, the SLD of the guest fluid, ρ_f , in accessible

pores can be changed by mixing hydrogenated and deuterated solvents, such as H_2O and D_2O , with different ratios [28] for neutron scattering or loading gas with different pressures for both x-ray and neutron scattering [33–35]. Thus, the GPSLM can be used for both SAXS and SANS, even though we use SANS as the example to demonstrate this method.

For heterogeneous systems, the general equation for Porod’s scattering can be written as

$$I(Q) \xrightarrow{Q \rightarrow \infty} 2\pi \frac{S_T}{V} \langle \Delta\rho^2 \rangle_s Q^{-4} = C_P Q^{-4}, \quad (2)$$

where $C_P = 2\pi \frac{S_T}{V} \langle \Delta\rho^2 \rangle_s$ is the Porod’s constant. C_P can be easily obtained by fitting the intensity in Porod’s law region with $I(Q) = C_P Q^{-4}$. The mean square deviation of the SLD (MSD_{SLD}), or $\langle \Delta\rho^2 \rangle_s$, in Eq. (2) is defined as

$$\langle \Delta\rho^2 \rangle_s \equiv \frac{1}{S_T} \int_S \Delta\rho(S)^2 dS. \quad (3)$$

Equation (3) integrates through all the interface S with the total interfacial area as S_T inside volume V of the sample. $\langle \Delta\rho^2 \rangle_s$ is thus the surface-averaged parameter instead of the volume-averaged one. Note that S_T includes both accessible and inaccessible interfaces. $\Delta\rho(S)$ is the SLD contrast between the components at different sides of the interface S . For accessible pores, $\Delta\rho(S) = \rho(S) - \rho_f$ since one side of interface S is an open pore accessible to the guest fluid with SLD as ρ_f , and the other side of S is the solid matrix with SLD as $\rho(S)$. For inaccessible interfaces between solid components of different SLD, $\Delta\rho(S)$ is the SLD difference of the solid matrix on the two sides of the interface S . For the special case of inaccessible empty pores, $\Delta\rho(S) = \rho(S)$.

When applying the contrast variation procedure, only $\langle \Delta\rho^2 \rangle_s$ (and thus C_P) is changed with the guest fluid SLD, ρ_f , in Eq. (2). It is therefore convenient to normalize the intensity to remove other constant terms, i.e., $2\pi Q^{-4} \frac{S_T}{V}$, at the same Q in the Porod’s scattering region. $R(\rho_f)$ is defined to be the ratio of C_P between the case when intensity $I(Q)$ is measured with the guest fluid SLD as ρ_f and the case for $I(Q)$ with $\rho_f = 0$, i.e.,

$$R(\rho_f) \equiv \frac{C_P(\rho_f)}{C_P(\rho_f = 0)} = \frac{\langle \Delta\rho^2 \rangle_{s,\rho_f}}{\langle \Delta\rho^2 \rangle_{s,\rho_f = 0}} = \frac{I(Q, \rho_f)}{I(Q, \rho_f = 0)}. \quad (4)$$

Equation (4) also shows that $R(\rho_f)$ can be obtained by simply taking the ratio of scattering intensity $I(Q)$ at a given Q value with guest solvent molecules and without guest solvent molecules if the intensity of Porod’s law scattering region is so strong that the background signal can be ignored.

We will demonstrate using five different situations from the simplest case, case 1, to the most general case, case 5, that in the Porod’s scattering region ($I(Q) \propto Q^{-4}$), the scattering intensity will reduce to Eq. (2) with different mathematical expressions of $\langle \Delta\rho^2 \rangle_s$. In addition, $R(\rho_f)$ for these five cases can all be expressed as a parabolic function of ρ_f written as

$$R(\rho_f) = \frac{1}{\rho_{2M}^2} (\rho_f - \rho_A)^2 + \Delta_H^2. \quad (5)$$

The coefficients ρ_A , ρ_{2M}^2 , and Δ_H^2 have different physical meanings in different cases. The detailed derivations of Eq. (5) in different cases can be found in Eqs. (A2), (B2), (C2), (D2),

and (E2) in Appendices A, B, C, D, and E, respectively. In general, ρ_A and ρ_{2M}^2 are related to the surface-averaged SLD and the second moment of matrix SLD, respectively, and Δ_H^2 is the heterogeneity parameter that is related to the surface heterogeneity of the materials. The minimum of the ratio, $R(\rho_f)_{\min}$, takes place at $\rho_f = \rho_{f,\min}$ and $R(\rho_f) = R(\rho_{f,\min})$. Based on Eq. (5), we have

$$\rho_{f,\min} = \rho_A, \quad (6)$$

$$R(\rho_{f,\min}) = \Delta_H^2. \quad (7)$$

By doing contrast variation and plotting $R(\rho_f)$ versus ρ_f , the values of ρ_A , Δ_H^2 , and ρ_{2M}^2 can be easily retrieved by experimentally searching for the SLD of the guest fluid at which $R(\rho_f)$ reaches its minimum. For the simplest case demonstrated in the previous study [26] (case 1 that will be described below), ρ_A is the surface-averaged SLD of the matrix and Δ_H^2 is the normalized mean square deviation of matrix SLD from ρ_A , or the surface heterogeneity.

The five cases with different levels of complexity being discussed in this study are illustrated in Figs. 1(b)–1(f). We try to incorporate as many types of porous materials as possible in this work. The solid matrices shown in Fig. 1 have different domains with SLD of $\rho(S)$ that depends on the interface S . Different SLDs are drawn in different colors. In Fig. 1, the dashed lines outline the interface that can be accessible to the guest fluid, i.e., one side of these dashed lines are open pores; the solid lines outline the inaccessible interface that fluid molecules cannot access to. The space outlined by solid lines can be either inaccessible pores or inaccessible compact solid pockets. The open pores are shown in the void space (the light green color) in between the domains. These open pores are accessible to the guest fluid whose SLD ρ_f can be changed by contrast variation. Within the solid domains, there might also be some very small pores with pore size much smaller than the length scale L of the Porod's scattering region ($L \approx \frac{2\pi}{Q}$). Due to the length scale difference, these small pores only “look like” part of the solid domains in the Porod's Q range and the domain SLD is the “average” SLD of the solid matrix and these small pores. Because these small pores can be either accessible or inaccessible to the guest fluid, the SLD of domain d , ρ_d can also be changed by the guest fluid. Here, we adopt a straightforward assumption:

$$\begin{aligned} \rho_d &= [1 - \varphi(S)]\rho(S) + \varphi(S)\rho_f \\ &= \varphi_m(S)\rho(S) + [1 - \varphi_m(S)]\rho_f. \end{aligned} \quad (8)$$

$\rho(S)$ is the solid matrix SLD that depends on the interface S due to the chemical heterogeneity of the material; $\varphi(S)$ and $\varphi_m(S) = 1 - \varphi(S)$ are the volume fraction of accessible small pores and solid matrix, respectively, within the domain. The inaccessible small pores are accounted as the solid matrix because their SLD is not changed by the guest fluid, just like solid. Different domain d may have different $\varphi(S)$ and $\varphi_m(S)$ because of the structure heterogeneity and ρ_d will have different dependence of ρ_f for each domain [Eq. (8)].

Depending on the cases, different parameters can be extracted. The mathematical forms and the extractable parameters are introduced individually for each case. The detailed

derivations of the formulas can be found in Appendices A, B, C, D, and E.

A. Case 1: All the pores are accessible and the SLD of the solid matrix is not changed by loading the guest fluid

This simplest case [case 1 shown in Fig. 1(b)] has been discussed in our previous study [26]. For the completeness of the discussion, we also include the main results of the simplest case here. In this case, all pores are accessible by the guest fluid and the SLD of the solid matrix is not affected by the loaded guest fluid. This situation is common for many synthetic porous materials, such as mesoporous silica or carbon [34,36]. The Porod's scattering from the mesopores is shown at the high Q region, if the background and other type of scattering feature are properly subtracted [37]. Mixture of different kinds of mesoporous materials forms a heterogeneous material whose Porod's scattering region at high Q can be analyzed using the method described in case 1.

For case 1, the contrast term can be written as Eq. (2) with $\langle \Delta\rho^2 \rangle_s$ written as

$$\langle \Delta\rho^2 \rangle_s = \frac{1}{S_T} \int_S [\rho(S) - \rho_f]^2 dS. \quad (9)$$

Therefore,

$$\begin{aligned} R(Q, \rho_f) &\equiv \frac{\frac{1}{S_T} \int_S [\rho(S) - \rho_f]^2 dS}{\frac{1}{S_T} \int_S \rho(S)^2 dS} \\ &= 1 - 2\rho_f \frac{\frac{1}{S_T} \int_S \rho(S) dS}{\frac{1}{S_T} \int_S \rho(S)^2 dS} + \rho_f^2 \frac{1}{\frac{1}{S_T} \int_S \rho(S)^2 dS} \\ &= 1 - 2\rho_f \frac{\rho_A}{\rho_{2M}^2} + \rho_f^2 \frac{1}{\rho_{2M}^2} \\ &= \frac{1}{\rho_{2M}^2} (\rho_f - \rho_A)^2 + 1 - \frac{\rho_A^2}{\rho_{2M}^2}. \end{aligned} \quad (10)$$

The intensity ratio $R(\rho_f)$ reduces to a parabolic function shown in Eq. (5) with the coefficients

$$\rho_A = \frac{1}{S_T} \int_S \rho(S) dS, \quad (11)$$

$$\rho_{2M}^2 = \frac{1}{S_T} \int_S \rho(S)^2 dS = \langle \Delta\rho^2 \rangle_{s, \rho_f=0}, \quad (12)$$

$$\Delta_H^2 = \frac{\rho_{2M}^2 - \rho_A^2}{\rho_{2M}^2} = \frac{\frac{1}{S_T} \int_S [\rho(S) - \rho_A]^2 dS}{\rho_{2M}^2}. \quad (13)$$

Equations (11) and (12) show that ρ_A and ρ_{2M}^2 are exactly the surface-averaged SLD and the surface-averaged second moment of the SLD. Δ_H is directly linked to the variation of the SLD along all pore surface [Eq. (13)]. ρ_A and Δ_H can be easily determined by finding the minimum of the parabolic function $R(\rho_f)$ and applying Eqs. (6) and (7). $\rho_{2M}^2 = \frac{\rho_A^2}{1 - \Delta_H^2}$ can then be calculated through ρ_A and Δ_H .

After obtaining ρ_A , Δ_H^2 , and ρ_{2M}^2 (and therefore $\langle \Delta\rho^2 \rangle_{s, \rho_f=0}$), the surface area to volume ratio, $\frac{S_T}{V}$, can be calculated through Eqs. (2) and (12) using the scattering data

at $\rho_f = 0$, i.e.,

$$\frac{S_T}{V} = \frac{Q^4 I(Q, \rho_f = 0)}{2\pi} \frac{1}{\rho_{2M}^2} = \frac{C_P(\rho_f = 0)}{2\pi} \frac{1}{\rho_{2M}^2}. \quad (14)$$

Since the total volume V seen by neutron and x ray is a known value from the experiment configuration, the total surface area S_T can be straightforwardly obtained.

By applying the commonly used contrast variation procedure, the GPSLM provides more information such as the surface heterogeneity (Δ_H^2) of the matrix SLD on all the interfaces relevant to the Porod's scattering length scale. GPSLM in case 1 was successfully applied to kerogens isolated from natural shale rocks and the results showed that isolated kerogen with higher maturity has larger ρ_A , i.e., smaller hydrogen content, and smaller Δ_H^2 , i.e., more homogeneous [26].

In addition, the GPSLM can provide a more accurate value of the surface-averaged SLD, ρ_A , and the total surface area, S_T . Note that the simple version of the Porod's scattering method [Eq. (1)] has been widely used for estimating ρ_A and S_T even though the results would be less accurate. Using the GPSLM, we can estimate the possible errors introduced by simply using Eq. (1). Equation (5) shows that when Δ_H^2 is small, i.e., $\Delta_H^2 \rightarrow 0$, or when ρ_f is very different from ρ_A , i.e., $(\rho_f - \rho_A)^2 \gg \rho_{2M}^2 \Delta_H^2$, the parabolic function $R(\rho_f)$ reduces to the homogeneous equation, i.e., $R(\rho_f) \rightarrow \frac{1}{\rho_{2M}^2}(\rho_f - \rho_A)^2$. Therefore, when one has some preknowledge of the approximate magnitude of ρ_A before an experiment, using the guest fluid with ρ_f far away from ρ_A to conduct contrast variation will allow more accurate determination of the real ρ_A if the traditional Porod's method is applied to the heterogeneous materials. In previous work [26], we simulated the scattering intensity of heterogeneous systems with known surface properties, i.e., known ρ_A and S_T , and analyzed the simulated data by Eq. (1). This allowed us to determine the surface heterogeneity effect on S_T and ρ_A . The results showed that even though we can determine accurate ρ_A by choosing ρ_f with $(\rho_f - \rho_A)^2 \gg \rho_{2M}^2 \Delta_H^2$, the traditional Porod's method still either overestimates or underestimates S_T , depending on the parameters used.

B. Case 2: There are some dead pores or solid pockets inaccessible to guest fluids, but the SLD of solid matrix is still not changed by loading guest fluid

This case [shown in Fig. 1(c)] may be common for synthetic porous materials using functional groups to do interface modification of the pores [38]. In this type of materials, the functional groups may detach from the pore surface or have inhomogeneous distribution on the pore surface and then block the pores. It is also viewed as a commonly encountered case in natural porous materials such as shales and coals [27]. Estimation of the exact amount of dead pores compared to accessible pores is still a challenging work. However, the surface properties of accessible pores are often the key factors to determine the storage and transport properties of guest molecules in this type of porous materials. The GPSLM still works for this case, but the interpretation of some parameters needs to include the dead pore information.

In this case, $\langle \Delta \rho^2 \rangle_s$ in Eq. (2) becomes

$$\langle \Delta \rho^2 \rangle_s = \frac{1}{S_T} \left\{ \int_{S_A} [\rho(S_A) - \rho_f]^2 dS_A + \int_{S_{NA}} [\rho(S_{NA}) - \rho_{NA}(S_{NA})]^2 dS_{NA} \right\}. \quad (15)$$

S_A represents the pore surfaces at which the pores can be accessed by the guest fluid. S_{NA} , where NA is the abbreviation for "nonaccessible," indicates the interfaces inaccessible by the guest fluid. $\rho(S_A)$ is the SLD of the pore walls that can be accessed by a guest fluid. $\rho_{NA}(S_{NA})$ and $\rho(S_{NA})$ are the values of the SLD on the two sides of inaccessible surface S_{NA} . $\rho_{NA}(S_{NA})$ can be the SLD of the compact solid pockets or dead pores that cannot be reached by the guest fluid because they are imbedded in the solid grain with the SLD of $\rho(S_{NA})$. It is noted that the total surface area, S_T , is the sum of the accessible surface area, S_A , and inaccessible surface area, S_{NA} , as

$$S_T = S_A + S_{NA}. \quad (16)$$

The second term in the square bracket of Eq. (15), i.e., the nonaccessible term, is a constant that does not vary with the guest fluid SLD ρ_f . We thus define

$$C_{NA} = \int_{S_{NA}} [\rho(S_{NA}) - \rho_{NA}(S_{NA})]^2 dS_{NA}. \quad (17)$$

The intensity ratio $IR(\rho_f)$ can also be written as Eq. (5) as a parabolic function of ρ_f . For case 2, the results are now expressed as

$$\rho_A = \frac{1}{S_A} \int_{S_A} \rho(S_A) dS_A, \quad (18)$$

$$\rho_{2M}^2 = \frac{1}{S_A} \left[\int_{S_A} \rho(S_A)^2 dS_A + C_{NA} \right] = \frac{S_T}{S_A} \langle \Delta \rho^2 \rangle_{s, \rho_f=0}, \quad (19)$$

$$\Delta_H^2 = \frac{\rho_{2M}^2 - \rho_A^2}{\rho_{2M}^2} = \frac{\frac{1}{S_A} \left\{ \int_{S_A} [\rho(S_A) - \rho_A]^2 dS_A + C_{NA} \right\}}{\rho_{2M}^2}. \quad (20)$$

It is important to point out that ρ_A for case 2 is the surface-averaged SLD integrated only over the "accessible" surface area S_A , not all the surface area. Therefore, the obtained average SLD is a surface-averaged value of the pores accessible to guest fluid. It does not contain any information of the interfaces inaccessible to the guest fluid. The heterogeneity parameter, Δ_H , still shows the surface heterogeneity of the accessible surface but needs to consider the contribution from C_{NA} [Eqs. (19) and (20)]. Thus, the extracted inhomogeneity information is also affected by inaccessible pore surfaces. ρ_{2M}^2 is the second moment parameter of the SLD that gives the average of the square of the SLD contrast at $\rho_f = 0$ per accessible surface area [Eq. (20)].

It is straightforward to determine the coefficients ρ_A and Δ_H^2 from the experimental data $R(\rho_f)$ using Eqs. (6) and (7). ρ_{2M}^2 can be calculated using $\rho_{2M}^2 = \frac{\rho_A^2}{1 - \Delta_H^2}$. Then the specific accessible surface area, $\frac{S_A}{V}$, can be obtained:

$$\frac{S_A}{V} = \frac{C_P(\rho_f = 0)}{2\pi} \frac{1}{\rho_{2M}^2}. \quad (21)$$

Because the scattering volume V is a known value, the accessible surface area S_A can now be determined. Note that the obtained surface area is not the total surface area S_T , but only includes the surface area accessible to the guest fluid.

The above results can lead to a very interesting observation. For a special situation of a homogeneous solid matrix with both dead pores and accessible pores, the GPSLM can now be used to quantify the amount of dead pores. For this special case, $\rho(S_A) = \rho(S_{NA}) = \rho_A = \rho_{f,\min}$ and $\rho_{NA}(S_{NA}) = 0$, which lead to $C_{NA} = \rho_A^2 S_{NA}$, $\rho_{2M}^2 = \frac{S_T}{S_A} \rho_A^2$, and $\Delta_H^2 = \frac{S_{NA}}{S_T}$. Therefore, after applying contrast variation, the minimum of $R(\rho_f)$, which gives ρ_A and Δ_H^2 of the homogeneous materials, provides the surface fraction of inaccessible surface area among the total surface area. This value is very difficult to obtain with any other method.

C. Case 3: All pores are accessible. The SLD of solid domains changes with the SLD of loading guest fluid. All the solid domains have the same dependence of average domain SLD on guest fluid SLD

Compared to case 1, case 3 [Fig. 1(d)] is applicable to the situations when the SLD of the solid matrix can change with the loading guest fluid. The change of the domain SLD with guest fluid is illustrated by the mesh drawn in Fig. 1(d). This can happen when there are lots of fluid-accessible small pores with size much smaller than the length scale L detectable by Porod's scattering region ($L \approx \frac{2\pi}{Q}$) and therefore Porod's scattering cannot distinguish the small pores from the solid matrix. As a result, the average SLD of domains changes with the SLD of the loading fluid, as shown in Eq. (8). In this case, the Porod's scattering is not sensitive to the surface of small pores, but only sensitive to the surface of large domains. In some works [39], the surface of large domains is called the "envelope" surface. As a simple example, the Porod's scattering from the grain boundaries of mesoporous materials shown at low Q region cannot pick up the mesopore structure because the size of the mesopores is too small compared with the Porod's scattering length scale L [33,34,40]. Case 3 can be applied to analyze the Porod's scattering region at low Q for a mixture of mesoporous materials composed of different chemical components.

In case 3, the volume fraction of accessible small pores is further assumed to be the same for all the different domains, i.e., $\varphi(S) = \varphi$ and $\varphi_m(S) = \varphi_m = 1 - \varphi$ in Eq. (8). Here the small pores not accessible to loading fluid and with size much smaller than L are considered as part of the solid matrix and contribute to φ_m instead of φ because their SLD is not changed with contrast variation.

In this case, $\langle \Delta\rho^2 \rangle_s$ in Eq. (2) can be expressed as

$$\langle \Delta\rho^2 \rangle_s = \left\{ \frac{\varphi_m^2}{S_T} \int_S [\rho(S) - \rho_f]^2 dS \right\}. \quad (22)$$

Equation (22) is very similar to Eq. (9) for case 1 except that $\langle \Delta\rho^2 \rangle_s$ is now weighted by the square of the matrix volume fraction in the domains, φ_m^2 . Note that the integration is over the "envelope" surface, i.e., the surface of large domains. Interestingly, $R(\rho_f)$ for case 3 still follows a parabolic function. Moreover, the parameters ρ_A and Δ_H^2 in $R(\rho_f)$ for case 3 have the same formulas as those for case 1, i.e.,

$\rho_A = \frac{1}{S_T} \int_S \rho(S) dS$ [Eq. (11)] and $\Delta_H^2 = \frac{\{\frac{1}{S_T} \int_S [\rho(S) - \rho_A]^2 dS\}}{\rho_{2M}^2}$ [Eq. (13)]. Therefore, when all the domains have the same volume fraction of small pores, the fact that the matrix may change its SLD due to the small pore filling inside the solid domains does not affect the conclusions that ρ_A is exactly the surface-averaged SLD and Δ_H is directly the variation of the SLD along the surface. The only difference is that in case 3, all the surface means the "envelope" surface relevant to the Porod's scattering length scale L , which does not include the surface of tiny pores in the solid matrix.

ρ_{2M}^2 is also similar to case 1 [Eq. (12)] except for its relation with $\langle \Delta\rho^2 \rangle_s$ (last equality):

$$\rho_{2M}^2 = \frac{1}{S_T} \int_S \rho(S)^2 dS = \frac{\rho_A^2}{1 - \Delta_H^2} = \frac{1}{\varphi_m^2} \langle \Delta\rho^2 \rangle_{s, \rho_f=0}. \quad (23)$$

Therefore, finding the minimum of $R(\rho_f)$ through contrast variation and applying the GPSLM allows one to determine the envelope surface average of the SLD (ρ_A), second moment of the SLD (ρ_{2M}^2), and heterogeneity parameter (Δ_H^2). In addition, combining Eqs. (2) and (23), the $\varphi_m^2 S_T$, i.e., the total surface area weighted by φ_m^2 , can be retrieved through

$$\frac{\varphi_m^2 S_T}{V} = \frac{C_P(\rho_f = 0)}{2\pi} \frac{1}{\rho_{2M}^2}. \quad (24)$$

It is worth pointing out in some special cases [39,41] when the Q range is wide enough to cover both length scales of tiny pores buried inside the large domains and the large domains themselves, the SANS pattern will contain two Porod's scattering regions: the low Q region (case 3) gives the surface heterogeneity information of the envelope surfaces and the high Q region (case 1) provides the surface heterogeneity of all the interfaces including both tiny pores and large domains.

D. Case 4: The SLD of solid domains have different dependence of average domain SLD on guest fluid SLD and all the pores with length scale larger than L are accessible

Case 4 [Fig. 1(e)] is similar to case 3, except that the domains have different volume fractions of the tiny pores accessible to the guest fluid, $\varphi(S)$. $\varphi(S)$ and $\varphi_m(S) = 1 - \varphi(S)$ now depend on which domain the surface S is located at. According Eq. (8), the S -dependent $\varphi(S)$ and $\varphi_m(S)$ result in different relations between the domain SLD, ρ_d , and the guest fluid SLD, ρ_f , for different domains d . The meshed patterns in Fig. 1(e) are therefore drawn differently for different domains. Case 4 can be applied to the synthetic porous materials composed of different chemical compounds which are not mixed well in space and result in different grains with different pore volume fractions.

In case 4, $\langle \Delta\rho^2 \rangle_s$ in Eq. (2) becomes

$$\langle \Delta\rho^2 \rangle_s = \left\{ \frac{1}{S_T} \left[\int_S \varphi_m(S)^2 \rho(S)^2 dS - 2\rho_f \int_S \varphi_m(S)^2 \rho(S) dS + \rho_f^2 \int_S \varphi_m(S)^2 dS \right] \right\}. \quad (25)$$

The $R(\rho_f)$ again follows the parabolic function as shown in Eq. (5). The results for different parameters are

$$\rho_A = \int_S f(\varphi_m) \rho(S) dS, \quad (26)$$

$$\rho_{2M}^2 = \int_S f(\varphi_m) \rho(S)^2 dS = \frac{S_T}{\int_S \varphi_m(S)^2 dS} \langle \Delta \rho^2 \rangle_{s, \rho_f=0}, \quad (27)$$

$$\Delta H^2 = \frac{\rho_{2M}^2 - \rho_A^2}{\rho_{2M}^2} = \frac{\left\{ \int_S f(\varphi_m) [\rho(S) - \rho_A]^2 dS \right\}}{\rho_{2M}^2}, \quad (28)$$

where $f(\varphi_m)$ is a probability density function that is defined as

$$f(\varphi_m) = \frac{\varphi_m(S)^2}{\int_S \varphi_m(S)^2 dS}, \quad \text{and} \quad (29)$$

$$\int_S f(\varphi_m) dS = 1. \quad (30)$$

$f(\varphi_m)dS$ is the probability of finding the square of the matrix volume fraction in the domains to be $\varphi_m(S)^2$ on a surface element, dS . Note that Eqs. (25)–(30) are all integrated through the “envelope” surface S .

Equations (26)–(28) for case 4 are similar to Eqs. (11)–(13) for the simplest case 1 except that all the integral is now weighted by the probability density function $f(\varphi_m)$. Therefore, the minimum of $R(\rho_f)$ gives the $f(\varphi_m)$ -weighted envelope surface-averaged SLD [Eqs. (6) and (26)] and the $f(\varphi_m)$ -weighted surface heterogeneity [Eqs. (7) and (28)]. ρ_{2M}^2 is the $f(\varphi_m)$ -weighted envelope surface-averaged second moment of the SLD and it can be easily obtained through $\rho_{2M}^2 = \frac{\rho_A^2}{1 - \Delta H^2}$ [Eqs. (27) and (28)]. After determining ρ_A , ΔH^2 , and ρ_{2M}^2 and combining Eqs. (2), (25), and (27), the intensity $I(Q)$ at the contrast point $\rho_f = 0$ can be used to retrieve the summation of the square of the matrix volume fraction of domains on the envelope surface, i.e., $\int_S \varphi_m(S)^2 dS$, if the total

volume V is known:

$$\frac{\int_S \varphi_m(S)^2 dS}{V} = \frac{C_P(\rho_f = 0)}{2\pi} \frac{1}{\rho_{2M}^2}. \quad (31)$$

Note that in this case, it is no longer possible to obtain the true surface area. From Eq. (31), the obtained value is a $\varphi_m(S)^2$ -weighted total envelope surface area (not including the surface area of the tiny pores with size much smaller than Porod’s scattering length scale L). Hence, unless we know the distribution function of the pore volume fraction in different domains, it is not possible to obtain the true surface area using scattering methods. As the result of Eq. (31), the domains with larger $\varphi_m(S)$ have larger contribution to the final value of the $\varphi_m(S)^2$ -weighted total envelope surface area.

E. Case 5: Solid domains have different dependence of average domain SLD on guest fluid SLD and there are inaccessible pores and solid pockets

The most general case 5 [Fig. 1(f)] adds additional structure complexity to case 4 [Fig. 1(e)] by including the presence of nonaccessible pores and compact solid pockets with size detectable in the Porod’s Q range, $L \approx \frac{2\pi}{Q}$. In this case, there are three kinds of interfaces relevant at the length scale L : (1) the accessible interface between the matrix and the guest pore fluid [S_A , shown by dashed lines in Fig. 1(f)]; (2) the nonaccessible interface between nonaccessible solid or pore and matrix [S_{NA-m} , shown by the solid line in Fig. 1(f)]; (3) the interface between the compact solid pocket and the guest pore fluid [S_{NA-f} , shown by the dotted line in Fig. 1(f)]. For the solid pocket with S_{NA-f} interface, the fluid cannot diffuse into the pocket and therefore the “interior” of the pocket is inaccessible to the fluid and the SLD of the pocket does not change with fluid loading. However, the periphery of the pocket can be accessed to the guest fluid. S_{NA-f} is different than S_A in the sense that both sides of S_A vary with loading fluid (one side is the matrix with lots of tiny accessible pores in length scale $\ll L$ and the other side is the open pore in length scale $\approx L$ accessible to the guest fluid). The total surface area is the summation of the three kinds of interfaces, i.e.,

$$S_T = S_A + S_{NA-m} + S_{NA-f}. \quad (32)$$

$\langle \Delta \rho^2 \rangle_s$ in Eq. (2) for case 5 is written as

$$\langle \Delta \rho^2 \rangle_s = \frac{1}{S_T} \left\{ \left[\int \varphi_m(S_A)^2 dS_A + C_1 \right] \rho_f^2 - 2 \left[\int \varphi_m(S_A)^2 \rho(S_A) dS_A + C_2 \right] \rho_f + \left[\int \varphi_m(S_A)^2 \rho(S_A)^2 dS_A + C_3 \right] \right\}. \quad (33)$$

In Eq. (33),

$$C_1 = \int [1 - \varphi_m(S_{NA-m})]^2 dS_{NA-m} + \int dS_{NA-f}, \quad (34)$$

$$C_2 = \int [1 - \varphi_m(S_{NA-m})][\rho(S_{NA-m}) * \varphi_m(S_{NA-m}) - \rho_{NA}(S_{NA-m})] dS_{NA-m} + \int \rho_{NA}(S_{d,NA-f}) dS_{NA-f}, \quad (35)$$

$$C_3 = \int [\rho(S_{NA-m}) * \varphi_m(S_{NA-m}) - \rho_{NA}(S_{NA-m})]^2 dS_{NA-m} + \int \rho_{NA}(S_{d,NA-f})^2 dS_{NA-f}. \quad (36)$$

The $R(\rho_f)$ is still a parabolic function as described in Eq. (5). The coefficients of Eq. (5) are formulated as follows:

$$\rho_A = \frac{\int f(\varphi_m) \rho(S_A) dS_A + C'_2}{1 + C'_1}, \quad (37)$$

$$\rho_{2M}^2 = \frac{\int f(\varphi_m) \rho(S_A)^2 dS_A + C'_3}{1 + C'_1} = \frac{S_T}{\int_{S_A} \varphi_m(S_A)^2 dS + C_1} (\Delta\rho^2)_{s, \rho_f=0}, \quad (38)$$

$$\Delta_H^2 = \frac{\rho_{2M}^2 - \rho_A^2}{\rho_{2M}^2} = \frac{[\int f(\varphi_m) \rho(S_A)^2 dS_A + C'_3] [1 + C'_1] - [\int f(\varphi_m) \rho(S_A) dS_A + C'_2]^2}{[\int f(\varphi_m) \rho(S_A)^2 dS_A + C'_3] [1 + C'_1]}. \quad (39)$$

In the above equations, $f(\varphi_m) dS_A$ is the probability of finding the square of the matrix volume fraction in the domains to be $\varphi_m(S_A)^2$ on all accessible interface S_A , i.e.,

$$f(\varphi_m) = \frac{\varphi_m(S_A)^2}{\int_{S_A} \varphi_m(S_A)^2 dS_A} \quad \text{and} \quad (40)$$

$$\int_{S_A} f(\varphi_m) dS_A = 1. \quad (41)$$

C'_1 , C'_2 , and C'_3 are C_1 , C_2 , and C_3 normalized by $\int_{S_A} \varphi_m(S_A)^2 dS_A$, i.e.,

$$C'_1 = \frac{C_1}{\int_{S_A} \varphi_m(S_A)^2 dS_A}, \quad (42)$$

$$C'_2 = \frac{C_2}{\int_{S_A} \varphi_m(S_A)^2 dS_A}, \quad (43)$$

$$C'_3 = \frac{C_3}{\int_{S_A} \varphi_m(S_A)^2 dS_A}. \quad (44)$$

Similarly, the minimum of $R(\rho_f)$ found by contrast variation gives ρ_A [Eqs. (6) and (37)] and Δ_H^2 [Eqs. (7) and (39)]. Moreover, by combining Eqs. (2) and (38) and scattering data at $\rho_f = 0$, we can obtain

$$\frac{\int_{S_A} \varphi_m(S_A)^2 dS + C_1}{V} = \frac{C_P(\rho_f = 0)}{2\pi} \frac{1}{\rho_{2M}^2}. \quad (45)$$

Because the porous materials of case 5 are so complicated, the values obtained by the GPSLM are not surprisingly complicated. However, if the probability density function of $f(\varphi_m)$ is known, the above results can be simplified further.

III. GPSLM DATA ANALYSIS PROCEDURE ILLUSTRATED FROM SIMULATED SMALL-ANGLE SCATTERING DATA

In our previous work [26], kerogens isolated from the natural shale rocks of different maturity were used as examples of the simplest case 1 to demonstrate the procedure of using GPSLM to extract surface heterogeneity of materials. Future works are still needed to apply the GPSLM to samples corresponding to cases 2–5.

Here a heterogeneous model system of compact solid matrix with inaccessible pores (case 2) is simulated and the corresponding theoretical scattering intensity is calculated. We use this model system (with known parameters) to demonstrate the data analysis procedure of the GPSLM and show

how to extract the parameters of ρ_A , Δ_H^2 , ρ_{2M}^2 , and $\frac{S_A}{V}$ from a scattering experiment.

In the simulated model system, four different kinds of particles with hollow cores and different shell SLDs are mixed to generate a heterogeneous system, as shown in Fig. 2(a). Each particle can be treated as a domain with the shell as the solid matrix in the material. The hollow cores [outlined by the solid lines in Fig. 2(a)] are inaccessible to the guest fluid and their SLDs are fixed as zero during contrast variation. The shells are compact solids without tiny pores so the guest fluid cannot penetrate through the shells and the shell SLDs are unchanged during the contrast variation experiment. However, the SLD contrast across the interface between the shell and the accessible pore (drawn as dashed lines) keeps changing with the loading fluid. The core radius r_c , the average shell radius $\langle r_s \rangle$, the polydispersity of shell radius σ_{r_s} , shell SLD ρ_s , and particle number density n for the different particles are listed in Table I. Note that the concentration of particles in Fig. 2(a) is not drawn to the real scale. Artificial constant incoherent background with random noise is added to the signal to simulate the likely outcome of real data. The scattering intensity $I(Q)$ for the heterogeneous system at different loading fluid SLDs, ρ_f , is calculated (details are given in Appendix F). Figure 2(b) plots several simulated intensity curves, which show clear Porod's scattering law region that follows $I(Q) \propto Q^{-4}$ (for $0.02 < Q < 0.57 \text{ \AA}^{-1}$). Fitting the scattering intensity at the Porod's scattering Q region with Eq. (2) allows us to determine the Porod's constant C_P . The ratio of C_P , $\frac{C_P(\rho_f)}{C_P(\rho_f=0)}$, gives the $R(\rho_f)$ at ρ_f [Eq. (4)].

Figure 2(c) plots $R(\rho_f)$ vs ρ_f and $R(\rho_f)$ is shown to be a parabolic function of ρ_f as predicted in Eq. (5). Note that the curve in Fig. 2(c) is obtained by fitting 161 simulated SANS patterns by systematically varying ρ_f from 0 to $8 \times 10^{-6} \text{ cm}^{-1}$. The minimum of $R(\rho_f)$ gives the values of ρ_A and Δ_H^2 [Eqs. (6) and (7)], as indicated in Fig. 2(c). In this case (an example of case 2), ρ_A represents the average SLD of the accessible surface [Eq. (18)] and Δ_H^2 is the heterogeneity parameter with contributions from both the surface heterogeneity of accessible interfaces and a constant C_{NA} due to the SLD contrast between the hollow cores and solid matrix [Eqs. (17) and (20)]. ρ_{2M}^2 can be easily calculated through $\rho_{2M}^2 = \frac{\rho_A^2}{1 - \Delta_H^2}$ [Eq. (19)] and in this special case it represents the SLD square for "all" the interfaces per accessible surface area (note that the cores are hollow so $C_{NA} = \int_{S_{NA}} \rho(S_{NA})^2 dS_{NA}$ [Eq. (17)] and $\rho_{2M}^2 = \frac{1}{S_A} [\int_S \rho(S)^2 dS]$ [Eq. (19)]. With ρ_{2M}^2 and $C_P(\rho_f = 0)$, the accessible surface area per unit volume, $\frac{S_A}{V}$, can be determined by Eq. (21). The extracted ρ_A , Δ_H^2 ,

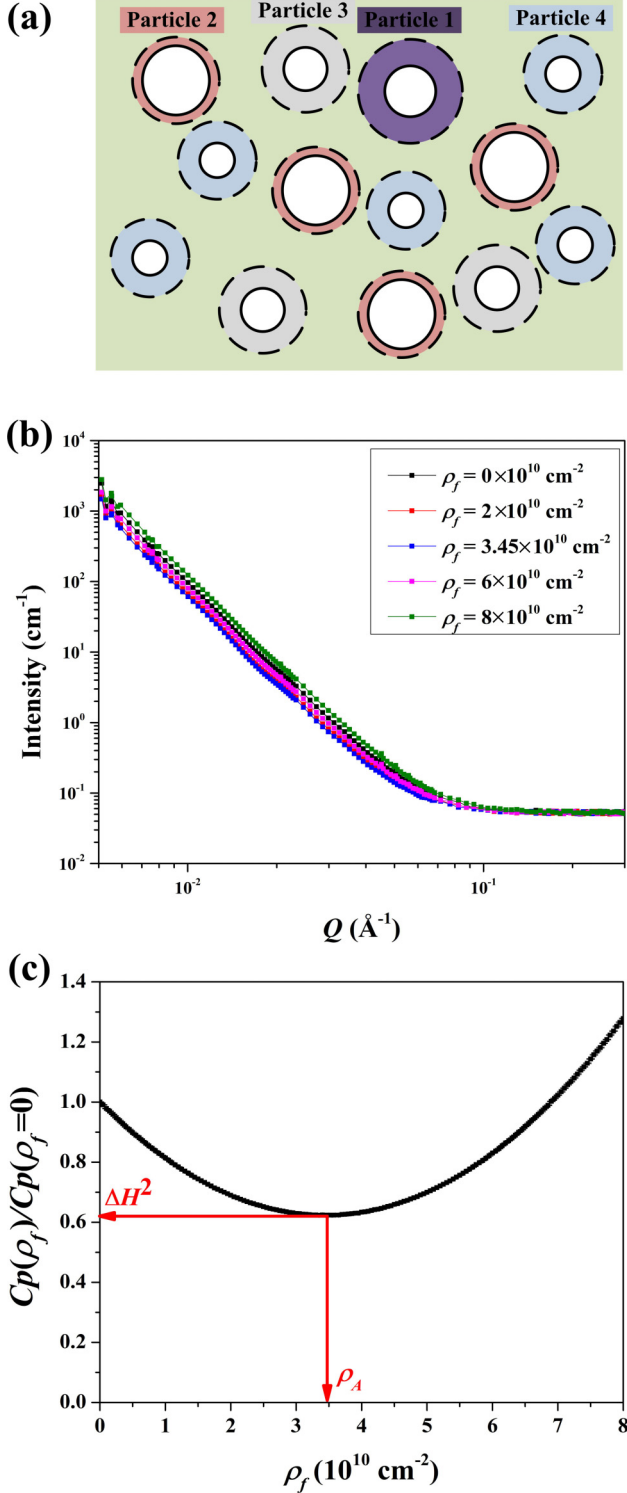


FIG. 2. (a) Illustration of the simulated heterogeneous model system. Different colors represent different SLDs. Solid and dashed curves outline the inaccessible and accessible interfaces, respectively, to the guest fluid (the continuous medium with green color). Particles have shells with different SLDs and hollow cores inaccessible to the fluid. The structure parameters of the four different kinds of particles are listed in Table I. (b) The simulated scattering intensity $I(Q)$ vs Q for the model system loaded with fluid of different SLDs, ρ_f . (c) $R(\rho_f) = \frac{C_p(\rho_f)}{C_p(\rho_f=0)}$ vs ρ_f for the model system with $C_p(\rho_f)$ as the Porod's constant obtained at guest fluid SLD = ρ_f using Eq. (2).

TABLE I. Structure parameters of the simulated model core-shell system illustrated in Fig. 2(a). Four kinds of core-shell particles with different shell scattering length densities (SLDs) and hollow cores are used for simulating heterogeneous compact domains with inaccessible pores (case 2). r_c , $\langle r_s \rangle$, σ_{r_s} , ρ_s , φ_p , and n are core radius, average shell radius, polydispersity of shell radius, SLD of the shell, volume fraction, and number density of each kind of particle, respectively.

Parameters	Particle 1	Particle 2	Particle 3	Particle 4
r_c (Å)	6000	8000	5000	4000
$\langle r_s \rangle$ (Å)	12000	10000	10000	9000
σ_{r_s} (Å)	1200	1000	1000	900
ρ_s (10^{14} m ⁻²)	7.44	6.30	1.00	0.40
φ_p	0.02	0.05	0.03	0.04
n (10^{15} m ⁻³)	2.76	11.94	7.16	13.10

ρ_{2M}^2 , and $\frac{S_A}{V}$ by analyzing the scattering intensity shown in Fig. 2(b) with the GPSLM, together with the corresponding theoretical known values, are listed in Table II. Table II clearly shows that GPSLM can faithfully retrieve the values of the essential surface parameters. Similar calculations can be made for particles with smaller sizes. The Porod's law region will shift to larger Q range. Two examples are given in Appendix F. Even though the estimation of $\frac{S_A}{V}$ is slightly different from the true value, it is mainly due to the slight oscillation of the form factors of spheres that cause a small deviation of scattering curves from a smooth Q^{-4} decay.

IV. DISCUSSIONS

For different cases discussed in this paper, the exact meaning of Δ_H varies slightly. But Δ_H is all related with the variation of the SLD along the interface in a sample. Therefore, we term Δ_H as the surface heterogeneity parameter. And the average scattering length density, ρ_A , is shown to be the accessible surface-averaged or related SLD for all cases. If two different fluids or gases can access different interfaces in a same sample, this difference can also be quantitatively evaluated by measuring the difference of ρ_A for different guest fluids or gases.

TABLE II. Exact values and experimental values of accessible specific surface area $\frac{S_A}{V}$, accessible-surface-averaged scattering length density (SLD) ρ_A , and surface-averaged second moment parameter ρ_{2M}^2 , and heterogeneity parameter Δ_H^2 . The exact structural parameters are directly calculated from the heterogeneous simulation system with known parameters described in Table I using the definition of Eqs. (17)-(19). The experiment parameters are extracted from GPSLM data analysis of simulated small-angle neutron scattering (SANS) intensity in Fig. 2(b).

Parameters	Exact	GPSLM (Simulation)
$\frac{S_A}{V}$ (m ⁻¹)	427535	460896 ± 621
ρ_A (10^{14} m ⁻²)	3.4496	3.4496 ± 0.0006
ρ_{2M}^2 (10^{28} m ⁻⁴)	31.56	31.57 ± 0.02
Δ_H^2	0.623	0.6230 ± 0.0001

Although we have tried to include as broad a range of scenarios as possible for the GPSLM, there are still some potential limitations due to the prerequisite of the presence of Porod's scattering feature in the scattering data, i.e., $I(Q) \propto Q^{-4}$. However, many materials have been shown to have scattering intensity with the power-law feature, but with the fractal exponent a not equal to 4, i.e., $I(Q) \propto Q^{-a}$ and $a \neq 4$ [42]. In these situations, if $a \approx 4$, we feel that the GPSLM should still serve as a good approximation and can be used to compare the surface heterogeneity among a series of samples with similar fractal exponents. If the exponent significantly deviates from 4 when a surface is not smooth with a fractal dimension, future works are needed to evaluate if the proposed method can be extended to surfaces with fractal dimensions.

In some systems, the Porod's scattering may be hidden by other scattering features with relatively large scattering intensity [37]. In this situation, the scattering pattern may not look like it has $I(Q) \propto Q^{-4}$ dependence. However, if Porod's scattering can be decoupled from other scattering features, the GPSLM can still be applied, as demonstrated in Fig. 2. The simplest and common example of this situation is the Porod's scattering hidden in a constant incoherent scattering at high Q region:

$$I(Q) = C_P(\rho_f) Q^{-4} + I_{\text{inc}}(\rho_f), \quad (46)$$

where $I_{\text{inc}}(\rho_f)$ is the incoherent scattering background, which usually depends on the SLD of the guest fluid. If $I_{\text{inc}}(\rho_f)$ can be properly determined and subtracted from the intensity, the GPSLM can be applied. It should be noticed, however, if the scattering at high Q region (Porod's scattering region) is very weak, the obtained results may have large error bars. In these cases, the accuracy of $I_{\text{inc}}(\rho_f)$ is very crucial for getting the meaningful surface heterogeneity parameter from Porod's scattering at high Q .

Another example that Porod's scattering can be decoupled from the rest of scattering is that there are some intrinsic structures in the system that do not change during the contrast variation. For example, the scattering can be due to the structure of components deeply buried inside the samples and not accessible to the guest fluid. For the simplicity of discussion, we only deal with the simple scattering form here as

$$I(Q) = I_P(Q) + I_f(Q) = C_P(\rho_f) Q^{-4} + C_f Q^{-a}. \quad (47)$$

$I_P(Q)$ represents Porod's scattering, which has the same mathematical expressions as described before and it changes with contrast variation. $I_f(Q)$ is the extra scattering from the same system, but does not change with the change of the guest fluid. One example is that $I_f(Q)$ can be due to some fractal structure that can be described as $C_f Q^{-a}$. a again is the fractal exponent and C_f is the fractal scattering prefactor; both are independent of the SLD of the guest fluid, ρ_f . To apply the GPSLM, the scattering intensity can be first subtracted by the minimum intensity at $\rho_f = \rho_{f,\text{min}}$, and the modified intensity can then be normalized to get the modified intensity ratio, i.e., $R_m(\rho_f)$:

$$\begin{aligned} R_m(\rho_f) &= \frac{I(Q, \rho_f) - I(Q, \rho_f = \rho_{f,\text{min}})}{I(Q, \rho_f = 0) - I(Q, \rho_f = \rho_{f,\text{min}})} \\ &= \frac{1}{\rho_A^2} (\rho_f - \rho_A)^2. \end{aligned} \quad (48)$$

The derivation of Eq. (48) can be found in Appendix G. Equation (48) shows that for scattering intensity as described by Eq. (47), where Porod's scattering can be decoupled from the rest of the scattering, one is still able to determine ρ_A by finding the ρ_f at the lowest modified intensity ratio, $R_m(\rho_f)$. Depending on the situations, the coefficient ρ_A has different formulas and physical meanings as for the five cases described above. However, information of the heterogeneity (Δ_H) and, consequently, the accessible surface area is lost and not able to be extracted using Eq. (48).

Note that when using SANS and SAXS to study the pore structure by loading gas into a sample, it is always good to check the difference pattern of the SANS and SAXS data within the Porod's scattering region, i.e., the difference of the scattering patterns before and after the gas is loaded. If the difference pattern has a different shape than the total scattering pattern, such as the change of the slope, this implies that part of the scattering features may be due to the scattering from some intrinsic structures in the material not affected by the gas loading. Thus, in order to analyze the pore structure of a system, it is more appropriate in this case to analyze the difference scattering pattern instead of the absolute scattering data.

The contrast variation method has been widely used for many decades. It is well known that if a material is not homogenous, the scattering pattern cannot be completely tuned to zero intensity for all Q ranges by simply varying the SLD of a guest solvent or gas. The residual scattering is due to the fact that different domains in a sample cannot be matched by the solvent or gas SLD simultaneously. Hence, it is not surprising that the residual scattering should contain some information of the heterogeneity of a material. Here, we demonstrate that if there is a Porod's scattering region for the SANS pattern, the residual scattering with the contrast variation method is exactly the surface heterogeneity parameter.

It is also important to emphasize that the average SLD, ρ_A , obtained by the contrast variation in the Porod's scattering region is the accessible surface-averaged SLD. In some cases, the accessible surface may have different SLD than the bulk materials. The GPSLM can provide the information for accessible surface areas only. In addition, if different liquids or gases can access different type of surfaces, the accessible surface-averaged SLD can provide some quantitative information of the difference of these different types of surfaces.

ρ_A is not the volume-averaged SLD that we typically think of, such as the Stuhmann's plot based on the Guinier scattering region. This indicates that the SLD of the solvent or gas needed to reach a minimum value for a sample can be different for different Q values. Thus, it is useful to examine theoretically the meaning of both ρ_A and Δ_H at other scattering regions, which may contain more information about the heterogenous distributions. Hence, the contrast variation method can provide us much more information other than an average SLD. And some future theoretical and experimental works are needed to fully realize the power of the contrast variation method to obtain more information from heterogeneous samples, which are very commonly encountered in different research areas.

The five cases discussed in this work all show that the scattering intensity at Porod's region is a parabolic function of the SLD of loading guest fluid, ρ_f [Eq. (5)]. This is a direct result

of the independence (case 1 and case 2) or linear dependence (case 3, case 4, and case 5) of the average domain SLD, ρ_d , on ρ_f [Eq. (8)]. We have not observed in our experiments that the intensity as a function of the SLD of the guest fluid does not follow a parabolic function. However, conceptually, the nonparabolic dependence of Porod's scattering intensity on ρ_f may appear when the average domain SLD is not linearly dependent on ρ_f , i.e., ρ_d does not follow Eq. (8). This situation, however, is beyond the scope of the current work.

V. CONCLUSIONS

In this study, we extend the generalized Porod's scattering law method (GPSLM) previously developed for a relatively simple case (case 1 described in this work) to a few more complicated cases of heterogeneous porous materials, which are commonly encountered in many man-made and natural porous materials. The applicability of GPSLM to five different classes of heterogeneous porous materials is fully discussed. The scattering intensity at Porod's scattering region for the discussed cases is all shown to be a parabolic function of the scattering length density (SLD) of the loading guest fluid, ρ_f [Eq. (5)].

The parameters of the parabolic function, ρ_A , ρ_{2M}^2 , and Δ_H^2 are related to the surface-averaged SLD, second moment of SLD, and the surface heterogeneity of the materials, respectively. These parameters can be easily determined from the minimum of the parabolic function [or simply fitting the parabolic function using Eq. (5)]. For different cases, the mathematical formulas and physical meanings of these parameters obtained by the GPSLM are rigorously derived and discussed. Even though there are many techniques that

can probe the surface heterogeneity information, it has been extremely challenging to obtain the heterogeneous information of porous materials noninvasively. The GPSLM is thus a powerful method to quantify the surface heterogeneity. It is worth noting that the surface heterogeneity parameter obtained from the GPSLM can be related to the variation of compositional properties of materials through the calculation of SLD. In addition, the GPSLM can provide the surface area more accurately compared with the classic Porod's law method applicable to mainly relatively homogeneous materials.

Overall, the GPSLM is a nondestructive and model-independent method that can be directly applied to bulk materials. It is based on the Porod's scattering law and the contrast variation, which are already commonly used in the scattering community. By combining these two methods, the GPSLM can extract more information. In general, the GPSLM can be applied to any system that can be carried out with the contrast variation procedure using either the mixture of hydrogenated and deuterated solvents or pressure change of gas. Therefore, the applicability of the GPSLM can cover a wide range of materials such as biomolecules, colloidal suspensions, multicomponent alloys, and cement pastes.

ACKNOWLEDGMENTS

This work was funded in part by Aramco Services Company. Y.L. acknowledges support by the Center for High Resolution Neutron Scattering (CHRNS), a partnership between the National Institute of Standards and Technology and the National Science Foundation under Agreement No. DMR-1508249.

APPENDIX A: DERIVATION OF GPSLM EQUATIONS FOR CASE 1

In case 1, all the pores are accessible by the guest fluid and the SLD of the solid matrix is not changed by loading the guest fluid. The intensity of case 1 at Porod's scattering Q range can be written as

$$I(Q, \rho_f) \xrightarrow{Q \rightarrow \infty} 2\pi \frac{S_T}{V} \langle \Delta \rho^2 \rangle_s Q^{-4} = 2\pi \frac{S_T}{V} \left\{ \frac{1}{S_T} \int_S [\rho(S) - \rho_f]^2 dS \right\} Q^{-4}. \quad (\text{A1})$$

The scattering intensity ratio between the intensity measured at the SLD of the guest fluid = ρ_f and the intensity measured at $\rho_f = 0$ can be derived:

$$\begin{aligned} R(Q, \rho_f) &\equiv \frac{I(Q, \rho_f)}{I(Q, \rho_f = 0)} = \frac{\frac{1}{S_T} \int_S [\rho(S) - \rho_f]^2 dS}{\frac{1}{S_T} \int_S \rho(S)^2 dS} = \frac{\frac{1}{S_T} [\int_S \rho(S)^2 dS - 2\rho_f \int_S \rho(S) dS + \rho_f^2 \int_S dS]}{\frac{1}{S_T} \int_S \rho(S)^2 dS} \\ &= 1 - 2\rho_f \frac{\frac{1}{S_T} \int_S \rho(S) dS}{\frac{1}{S_T} \int_S \rho(S)^2 dS} + \rho_f^2 \frac{1}{\frac{1}{S_T} \int_S \rho(S)^2 dS} = 1 - 2\rho_f \frac{\rho_A}{\rho_{2M}^2} + \rho_f^2 \frac{1}{\rho_{2M}^2} = \frac{1}{\rho_{2M}^2} (\rho_f - \rho_A)^2 + 1 - \frac{\rho_A^2}{\rho_{2M}^2} \\ &= \frac{1}{\rho_{2M}^2} (\rho_f - \rho_A)^2 + \Delta_H^2 = R(\rho_f). \end{aligned} \quad (\text{A2})$$

Equation (A2) proves that the intensity ratio of case 1 is a parabolic function of ρ_f that can be formulated as Eq. (5). The coefficients of the parabolic function, ρ_A , ρ_{2M}^2 , and Δ_H^2 are expressed in Eqs. (11)–(13).

At $\rho_f = 0$, $I(Q, \rho_f = 0) = 2\pi \frac{S_T}{V} [\frac{1}{S_T} \int_S \rho(S)^2 dS] Q^{-4} = 2\pi \frac{S_T}{V} \rho_{2M}^2 Q^{-4}$ and, therefore, $\frac{S_T}{V} = \frac{Q^4 I(Q, \rho_f = 0)}{2\pi} \frac{1}{\rho_{2M}^2}$, which gives Eq. (13) to calculate the specific surface area, $\frac{S_T}{V}$. Note that $Q^4 I(Q, \rho_f = 0) = C_P(\rho_f = 0)$.

APPENDIX B: DERIVATION OF GPSLM EQUATIONS FOR CASE 2

In case 2, some dead pores and compact solid pockets are inaccessible to the guest fluid, but the SLD of the solid matrix is still not changed by loading the guest fluid. The intensity at Porod's scattering region for case 2 is

$$I(Q, \rho_f) \xrightarrow{Q \rightarrow \infty} 2\pi \frac{S_T}{V} \langle \Delta \rho^2 \rangle_s Q^{-4} = 2\pi \frac{S_T}{V} \left(\frac{1}{S_T} \left\{ \int_{S_A} [\rho(S_A) - \rho_f]^2 dS_A + \int_{S_{NA}} [\rho(S_{NA}) - \rho_{NA}(S_{NA})]^2 dS_{NA} \right\} \right) Q^{-4}. \quad (\text{B1})$$

The scattering intensity ratio is

$$\begin{aligned} R(Q, \rho_f) &\equiv \frac{I(Q, \rho_f)}{I(Q, \rho_f = 0)} = \frac{\frac{1}{S_T} \{ \int_{S_A} [\rho(S_A) - \rho_f]^2 dS_A + \int_{S_{NA}} [\rho(S_{NA}) - \rho_{NA}(S_{NA})]^2 dS_{NA} \}}{\frac{1}{S_T} \{ \int_{S_A} \rho(S_A)^2 dS_A + \int_{S_{NA}} [\rho(S_{NA}) - \rho_{NA}(S_{NA})]^2 dS_{NA} \}} \\ &= \frac{\frac{1}{S_A} [\int_{S_A} \rho(S_A)^2 dS_A + C_{NA} - 2\rho_f \int_{S_A} \rho(S_A) dS_A + \rho_f^2 \int_{S_A} dS_A]}{\frac{1}{S_A} [\int_{S_A} \rho(S_A)^2 dS_A + C_{NA}]} \\ &= 1 - 2\rho_f \frac{\frac{1}{S_A} [\int_{S_A} \rho(S_A) dS_A]}{\frac{1}{S_A} [\int_{S_A} \rho(S_A)^2 dS_A + C_{NA}]} + \rho_f^2 \frac{1}{\frac{1}{S_A} [\int_{S_A} \rho(S_A)^2 dS_A + C_{NA}]} \\ &= 1 - 2\rho_f \frac{\rho_A}{\rho_{2M}^2} + \rho_f^2 \frac{1}{\rho_{2M}^2} = \frac{1}{\rho_{2M}^2} (\rho_f - \rho_A)^2 + \Delta_H^2 = R(\rho_f). \end{aligned} \quad (\text{B2})$$

Equation (B2) above reduces to the general parabolic function described in Eq. (5) with the coefficients, ρ_A , ρ_{2M}^2 , and Δ_H^2 , formulated as Eqs. (18)–(20).

At $\rho_f = 0$, $I(Q, \rho_f = 0) = 2\pi \frac{S_T}{V} \{ \frac{S_A}{S_T} \frac{1}{S_A} [\int_{S_A} \rho(S_A)^2 dS_A + C_{NA}] \} Q^{-4} = 2\pi \frac{S_A}{V} \rho_{2M}^2 Q^{-4}$ and, therefore, gives the accessible specific surface area $\frac{S_A}{V} = \frac{C_P(\rho_f=0)}{2\pi} \frac{1}{\rho_{2M}^2}$ in Eq. (21).

APPENDIX C: DERIVATION OF GPSLM EQUATIONS FOR CASE 3

In case 3, the solid domains have the same dependence of the average domain SLD, ρ_d , on the guest fluid SLD, ρ_f , and all the pores with length scale comparable to L are accessible. By setting a constant volume fraction of solid matrix as φ_m in Eq. (8), we get $\rho_d(S) = \varphi_m \rho(S) + (1 - \varphi_m) \rho_f$.

The Porod's scattering can be expressed as

$$\begin{aligned} I(Q, \rho_f) &\xrightarrow{Q \rightarrow \infty} 2\pi \frac{S_T}{V} \langle \Delta \rho^2 \rangle_s Q^{-4} \\ &= 2\pi \frac{S_T}{V} \left\{ \frac{1}{S_T} \int_S [\rho_d(S) - \rho_f]^2 dS \right\} Q^{-4} = 2\pi \frac{S_T}{V} \left\{ \frac{1}{S_T} \int_S [\varphi_m \rho(S) + (1 - \varphi_m) \rho_f - \rho_f]^2 dS \right\} Q^{-4} \\ &= 2\pi \frac{S_T}{V} \left\{ \frac{\varphi_m^2}{S_T} \int_S [\rho(S) - \rho_f]^2 dS \right\} Q^{-4}. \end{aligned} \quad (\text{C1})$$

Therefore, $\langle \Delta \rho^2 \rangle_s = \frac{\varphi_m^2}{S_T} \int_S [\rho(S) - \rho_f]^2 dS$ as described in Eq. (22).

$$R(Q, \rho_f) \equiv \frac{I(Q, \rho_f)}{I(Q, \rho_f = 0)} = \frac{\frac{\varphi_m^2}{S_T} \int_S (\rho(S) - \rho_f)^2 dS}{\frac{\varphi_m^2}{S_T} \int_S \rho(S)^2 dS} = \frac{\frac{1}{S_T} \int_S (\rho(S) - \rho_f)^2 dS}{\frac{1}{S_T} \int_S \rho(S)^2 dS}. \quad (\text{C2})$$

Equation (C2) reduces to Eq. (A2) as in case 1. Therefore, the coefficients for the parabolic function ρ_A , ρ_{2M}^2 , and Δ_H^2 have the same expressions as case 1 too, i.e., Eqs. (11)–(13).

At $\rho_f = 0$, $I(Q, \rho_f = 0) = 2\pi \frac{\varphi_m^2 S_T}{V} [\frac{1}{S_T} \int_S \rho(S)^2 dS] Q^{-4}$ and, therefore, $\frac{\varphi_m^2 S_T}{V} = \frac{C_P(\rho_f=0)}{2\pi} \frac{1}{\rho_{2M}^2}$ [Eq. (24)]. In case 3, we can only determine the total surface area weighted by the square of matrix volume fraction, $\varphi_m^2 S_T$.

APPENDIX D: DERIVATION OF GPSLM EQUATIONS FOR CASE 4

In case 4, the solid domains have different dependence of ρ_d on ρ_f and all the pores with length scale comparable to L are accessible. The matrix and pore volume fractions are not constant for different domains and Eq. (8) is used to describe ρ_d . The Porod's scattering can be expressed as

$$\begin{aligned} I(Q) &\xrightarrow{Q \rightarrow \infty} 2\pi \frac{S_T}{V} \langle \Delta \rho^2 \rangle_s Q^{-4} \\ &= 2\pi \frac{S_T}{V} \left\{ \frac{1}{S_T} \int_S [\rho_d(S) - \rho_f]^2 dS \right\} Q^{-4} = 2\pi \frac{S_T}{V} \left(\frac{1}{S_T} \int_S \{ \varphi_m(S) \rho(S) + [1 - \varphi_m(S)] \rho_f - \rho_f \}^2 dS \right) Q^{-4} \\ &= 2\pi \frac{S_T}{V} \left\{ \frac{1}{S_T} \int_S \varphi_m(S)^2 [\rho(S) - \rho_f]^2 dS \right\} Q^{-4}. \end{aligned} \quad (\text{D1})$$

Therefore, we can obtain $\langle \Delta \rho^2 \rangle_s$ as described in Eq. (24),

$$\begin{aligned}
 R(Q, \rho_f) &\equiv \frac{I(Q, \rho_f)}{I(Q, \rho_f = 0)} = \frac{\frac{1}{S_T} \int_S \varphi_m(S)^2 [\rho(S) - \rho_f]^2 dS}{\frac{1}{S_T} \int_S \varphi_m(S)^2 \rho(S)^2 dS} = 1 - 2\rho_f \frac{\frac{1}{S_T} \int_S \varphi_m(S)^2 \rho(S) dS}{\frac{1}{S_T} \int_S \varphi_m(S)^2 \rho(S)^2 dS} + \rho_f^2 \frac{\frac{1}{S_T} \int_S \varphi_m(S)^2 dS}{\frac{1}{S_T} \int_S \varphi_m(S)^2 \rho(S)^2 dS} \\
 &= 1 - 2\rho_f \frac{\frac{\frac{1}{S_T} \int_S \varphi_m(S)^2 \rho(S) dS}{\frac{1}{S_T} \int_S \varphi_m(S)^2 dS}}{\frac{\frac{1}{S_T} \int_S \varphi_m(S)^2 \rho(S)^2 dS}{\frac{1}{S_T} \int_S \varphi_m(S)^2 dS}} + \rho_f^2 \frac{\frac{\frac{1}{S_T} \int_S \varphi_m(S)^2 dS}{\frac{1}{S_T} \int_S \varphi_m(S)^2 dS}}{\frac{\frac{1}{S_T} \int_S \varphi_m(S)^2 \rho(S)^2 dS}{\frac{1}{S_T} \int_S \varphi_m(S)^2 dS}} = 1 - 2\rho_f \frac{\int_S f(\varphi_m) \rho(S) dS}{\int_S f(\varphi_m) \rho(S)^2 dS} + \rho_f^2 \frac{1}{\int_S f(\varphi_m) \rho(S)^2 dS} \\
 &= 1 - 2\rho_f \frac{\rho_A}{\rho_{2M}^2} + \rho_f^2 \frac{1}{\rho_{2M}^2} = \frac{1}{\rho_{2M}^2} (\rho_f - \rho_A)^2 + \Delta_H^2 = R(\rho_f). \tag{D2}
 \end{aligned}$$

The derivation in Eq. (D2) again reduces to the general parabolic function described in Eq. (5). The coefficients ρ_A , ρ_{2M}^2 , and Δ_H^2 for case 4 are indicated in Eqs. (26)–(28).

At $\rho_f = 0$, $I(Q, \rho_f = 0) = 2\pi \frac{S_T}{V} [\frac{1}{S_T} \int_S \varphi_m(S)^2 \rho(S)^2 dS] Q^{-4} = 2\pi \frac{[\frac{1}{S_T} \int_S \varphi_m(S)^2 dS] S_T}{V} [\frac{\frac{1}{S_T} \int_S \varphi_m(S)^2 \rho(S)^2 dS}{\frac{1}{S_T} \int_S \varphi_m(S)^2 dS}] Q^{-4} = 2\pi \frac{\int_S \varphi_m(S)^2 dS}{V} \rho_{2M}^2 Q^{-4}$. Therefore, for case 4, we can determine the specific surface area weighted by the square of the matrix volume fraction at each surface position, i.e., $\frac{\int_S \varphi_m(S)^2 dS}{V} = \frac{C_P(\rho_f=0)}{2\pi} \frac{1}{\rho_{2M}^2}$ as described in Eq. (31).

APPENDIX E: DERIVATION OF GPSLM EQUATIONS FOR CASE 5

In case 5, the solid domains have different dependence of ρ_d on ρ_f and there are inaccessible pores or compact solid pockets with length scale comparable to L . This is the most general case and we consider three different kinds of interfaces: (1) the accessible interface S_A between the open pore and the matrix domain whose average SLD can change with ρ_f ; (2) the interface S_{NA-m} between the nonaccessible pore or compact solid pocket whose SLD will not change with ρ_f and the matrix domain; (3) the interface S_{NA-f} between the nonaccessible solid pocket and the open pore. The average domain SLD, $\rho_d(S)$, again changes with ρ_f according to Eq. (8).

The Porod's scattering can be written as

$$\begin{aligned}
 I(Q) &\xrightarrow{Q \rightarrow \infty} 2\pi \frac{S_T}{V} \langle \Delta \rho^2 \rangle_s Q^{-4} \\
 &= 2\pi \frac{S_T}{V} \left(\frac{1}{S_T} \left\{ \int_{S_A} [\rho_d(S_A) - \rho_f]^2 dS_A + \int_{S_{NA-m}} [\rho_d(S_{NA-m}) - \rho_{NA}(S_{NA-m})]^2 dS_{NA-m} + \int_{S_{NA-f}} [\rho_{NA}(S_{NA-f}) - \rho_f]^2 dS_{NA-f} \right\} \right) Q^{-4} \\
 &= 2\pi \frac{S_T}{V} \left[\frac{1}{S_T} \left(\int_{S_A} \varphi_m(S_A)^2 [\rho(S_A) - \rho_f]^2 dS_A + \int_{S_{NA-m}} \{ \varphi_m(S_{NA-m}) \rho(S_{NA-m}) + [1 - \varphi_m(S_{NA-m})] \rho_f - \rho_{NA}(S_{NA-m}) \}^2 dS_{NA-m} \right. \right. \\
 &\quad \left. \left. + \int_{S_{NA-f}} [\rho_{NA}(S_{NA-f}) - \rho_f]^2 dS_{NA-f} \right) \right] Q^{-4} \\
 &= 2\pi \frac{S_T}{V} \frac{1}{S_T} \left(\left\{ \int_{S_A} \varphi_m(S_A)^2 \rho(S_A)^2 dS_A + \int_{S_{NA-m}} [\varphi_m(S_{NA-m}) \rho(S_{NA-m}) - \rho_{NA}(S_{NA-m})]^2 dS_{NA-m} + \int_{S_{NA-f}} \rho_{NA}(S_{NA-f})^2 dS_{NA-f} \right\} \right. \\
 &\quad \left. - 2\rho_f \left\{ \int_{S_A} \varphi_m(S_A)^2 \rho(S_A) dS_A + \int_{S_{NA-m}} [1 - \varphi_m(S_{NA-m})] [\rho_{NA}(S_{NA-m}) - \varphi_m(S_{NA-m}) \rho(S_{NA-m})] dS_{NA-m} \right. \right. \\
 &\quad \left. \left. + \int_{S_{NA-f}} \rho_{NA}(S_{NA-f}) dS_{NA-f} \right\} + \rho_f^2 \left\{ \int_{S_A} \varphi_m(S_A)^2 dS_A + \int_{S_{NA-m}} [1 - \varphi_m(S_{NA-m})]^2 dS_{NA-m} + \int_{S_{NA-f}} dS_{NA-f} \right\} \right) Q^{-4} \\
 &= 2\pi \frac{S_T}{V} \frac{1}{S_T} \left\{ \rho_f^2 \left[\int_{S_A} \varphi_m(S_A)^2 dS_A + C_1 \right] - 2\rho_f \left[\int_{S_A} \varphi_m(S_A)^2 \rho(S_A) dS_A + C_2 \right] + \left[\int_{S_A} \varphi_m(S_A)^2 \rho(S_A)^2 dS_A + C_3 \right] \right\} Q^{-4}. \tag{E1}
 \end{aligned}$$

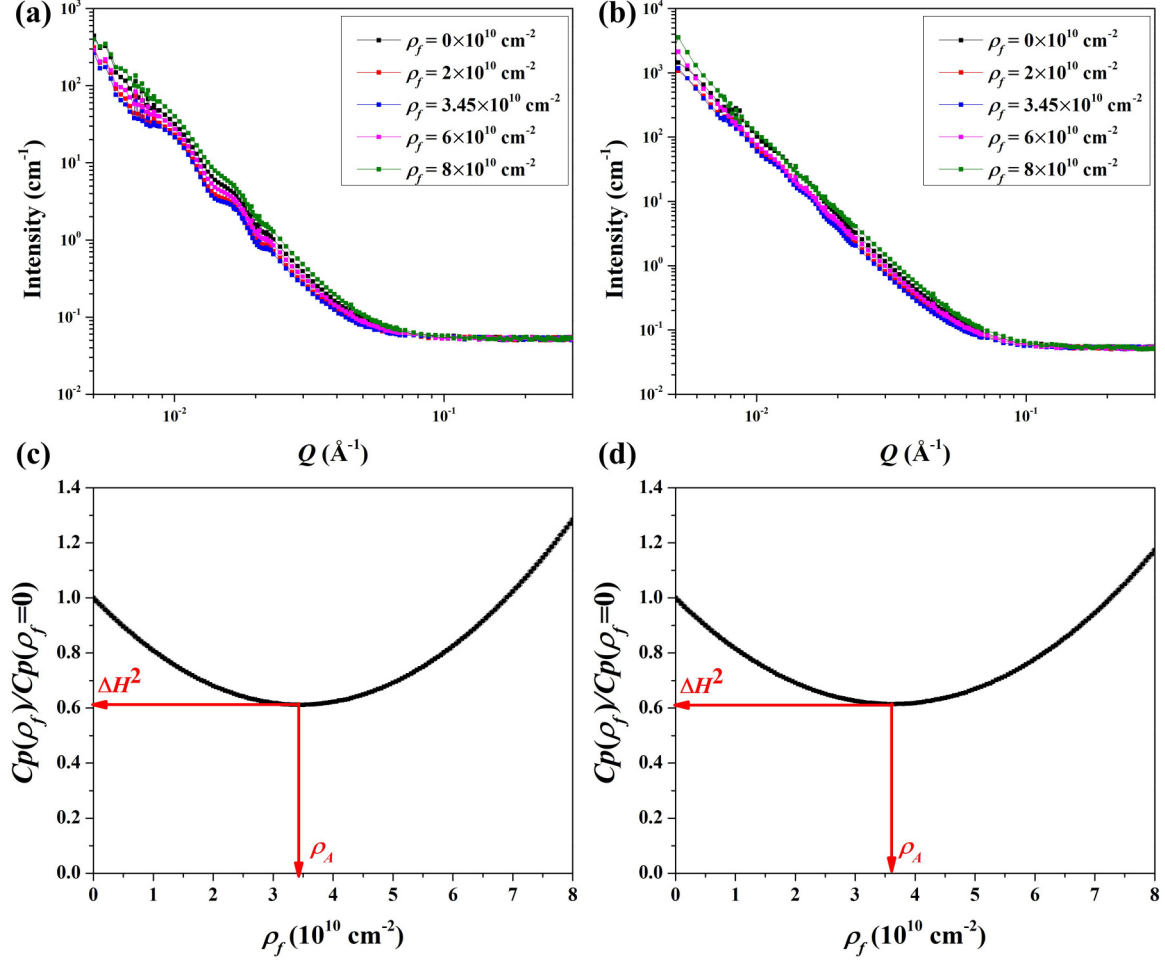


FIG. 3. (a) The simulated scattering intensity $I(Q)$ vs Q for the model system (sample 1) loaded with fluid of different SLDs, ρ_f . The structure parameters of the four different kinds of particles are listed in Table III. (b) The simulated scattering intensity $I(Q)$ vs Q for the model system (sample 2) loaded with fluid of different SLDs, ρ_f . The structure parameters of the four different kinds of particles are listed in Table IV. (c) $R(\rho_f) = \frac{C_p(\rho_f)}{C_p(\rho_f=0)}$ vs ρ_f for the model system with $C_p(\rho_f)$ as the Porod's constant obtained at guest fluid SLD = ρ_f using Eq. (2) for sample 1. (d) $R(\rho_f) = \frac{C_p(\rho_f)}{C_p(\rho_f=0)}$ vs ρ_f for the model system with $C_p(\rho_f)$ as the Porod's constant obtained at guest fluid SLD = ρ_f using Eq. (2) for sample 2.

This ends up with the complicated formula of $\langle \Delta \rho^2 \rangle_s$ shown in Eq. (33) of the main text,

$$\begin{aligned}
 R(Q, \rho_f) &\equiv \frac{I(Q, \rho_f)}{I(Q, \rho_f = 0)} = \frac{[\int_{S_A} \varphi_m(S_A)^2 \rho(S_A)^2 dS_A + C_3] - 2\rho_f [\int_{S_A} \varphi_m(S_A)^2 \rho(S_A) dS_A + C_2] + \rho_f^2 [\int_{S_A} \varphi_m(S_A)^2 dS_A + C_1]}{[\int_{S_A} \varphi_m(S_A)^2 \rho(S_A)^2 dS_A + C_3]} \\
 &= 1 - 2\rho_f \frac{\frac{[\int_{S_A} \varphi_m(S_A)^2 \rho(S_A) dS_A + C_2]}{\int_{S_A} \varphi_m(S_A)^2 dS_A}}{\frac{[\int_{S_A} \varphi_m(S_A)^2 \rho(S_A)^2 dS_A + C_3]}{\int_{S_A} \varphi_m(S_A)^2 dS_A}} + \rho_f^2 \frac{\frac{[\int_{S_A} \varphi_m(S_A)^2 dS_A + C_1]}{\int_{S_A} \varphi_m(S_A)^2 dS_A}}{\frac{[\int_{S_A} \varphi_m(S_A)^2 \rho(S_A)^2 dS_A + C_3]}{\int_{S_A} \varphi_m(S_A)^2 dS_A}} \\
 &= 1 - 2\rho_f \frac{[\int_{S_A} f(\varphi_m) \rho(S_A) dS_A + C_2']}{[\int_{S_A} f(\varphi_m) \rho(S_A)^2 dS_A + C_3']} + \rho_f^2 \frac{[1 + C_1']}{[\int_{S_A} f(\varphi_m) \rho(S_A)^2 dS_A + C_3']} \\
 &= 1 - 2\rho_f \frac{\frac{[\int_{S_A} f(\varphi_m) \rho(S_A) dS_A + C_2']}{[1 + C_1']}}{\frac{[\int_{S_A} f(\varphi_m) \rho(S_A)^2 dS_A + C_3']}{[1 + C_1']}} + \rho_f^2 \frac{1}{\frac{[\int_{S_A} f(\varphi_m) \rho(S_A)^2 dS_A + C_3']}{[1 + C_1']}} \\
 &= 1 - 2\rho_f \frac{\rho_A}{\rho_{2M}^2} + \rho_f^2 \frac{1}{\rho_{2M}^2} = \frac{1}{\rho_{2M}^2} (\rho_f - \rho_A)^2 + \Delta_H^2 = R(\rho_f). \tag{E2}
 \end{aligned}$$

We can see that even for the most complicated case 5, the intensity ratio $R(\rho_f)$ reduces to the same general equation, Eq. (5), with the coefficients ρ_A , ρ_{2M}^2 , and Δ_H^2 defined as Eqs. (37)–(39).

TABLE III. Information for sample 1. Four kinds of core-shell particles with different shell scattering length densities (SLDs) and hollow cores are used for simulating heterogeneous compact domains with inaccessible pores. r_c , $\langle r_s \rangle$, σ_{r_s} , ρ_s , φ_p , and n are core radius, average shell radius, polydispersity of shell radius, SLD of the shell, volume fraction, and number density of each kind of particle, respectively.

Parameters	Particle 1	Particle 2	Particle 3	Particle 4
r_c (Å)	2000	2667	1667	1333
$\langle r_s \rangle$ (Å)	4000	3333	3333	3000
σ_{r_s} (Å)	400	333	333	300
ρ_s (10^{14} m^{-2})	7.44	6.30	1.00	0.40
φ_p	0.002	0.005	0.003	0.004
n (10^{15} m^{-3})	7.46	32.23	19.34	35.37

$$\text{At } \rho_f = 0, \quad I(Q, \rho_f = 0) = 2\pi \frac{S_T}{V} \frac{1}{S_T} [\int_{S_A} \varphi_m(S_A)^2 \rho(S_A)^2 dS_A + C_3] \quad Q^{-4} = 2\pi \frac{[\int_{S_A} \varphi_m(S_A)^2 dS_A][1+C_1]}{V} \rho_{2M}^2 Q^{-4} = 2\pi \frac{[\int_{S_A} \varphi_m(S_A)^2 dS_A + C_1]}{V} \rho_{2M}^2 Q^{-4}.$$

In case 5, a specific surface area weighted by different factors, depending on the interface, can be determined: $\frac{[\int_{S_A} \varphi_m(S_A)^2 dS_A + C_1]}{V} = \frac{[\int_{S_A} \varphi_m(S_A)^2 dS_A + \int_{S_{NA-m}} (1-\varphi_m(S_{NA-m}))^2 dS_{NA-m} + \int_{S_{NA-f}} dS_{NA-f}]}{V} = \frac{[\int_{S_A} \varphi_m(S_A)^2 dS_A + \int_{S_{NA-m}} \varphi(S_{NA-m})^2 dS_{NA-m} + \int_{S_{NA-f}} dS_{NA-f}]}{V} = \frac{C_P(\rho_f=0)}{2\pi} \frac{1}{\rho_{2M}^2}$, which gives Eq. (44).

APPENDIX F: CALCULATION OF SCATTERING INTENSITY OF SIMULATED HETEROGENEOUS CORE-SHELL SYSTEM

Here we demonstrate how to calculate the scattering intensity $I(Q)$ of the simulated core-shell system described in Fig. 2(a) and Table I. The heterogeneous system is composed of four kinds of core-shell hollow particles with different size (different hollow core radius R_c , average shell radius $\langle R_s \rangle$, the polydispersity of shell radius σ_{R_s}) and different shell SLD, ρ_s . We can treat the shells as different compact domains that fluid molecules cannot penetrate through and the hollow cores are the inaccessible dead pores. The voids between the particles are accessible to the fluid. In this case, the Porod's law scattering region is at relatively high Q compared with the first diffraction peak of the interparticle structure factor, and we can ignore the interparticle structure factor, i.e., $S(Q) \approx 1$.

$P_i(Q)$ is the form factor of core-shell particle type i with core radius as $r_{c,i}$, shell radius as $r_{s,i}$, core SLD as $\rho_{c,i}$, and shell SLD as $\rho_{s,i}$. ρ_f is the SLD of the guest fluid.

$$P_i(Q, r_{c,i}, r_{s,i}, \rho_{c,i}, \rho_{s,i}, \rho_f) = \left[3 \left(\frac{4}{3} \pi r_{c,i}^3 \right) \frac{(\rho_{c,i} - \rho_{s,i})}{Q r_{c,i}} \left(\frac{\sin(Q r_{c,i})}{(Q r_{c,i})^2} - \frac{\cos(Q r_{c,i})}{Q r_{c,i}} \right) + 3 \left(\frac{4}{3} \pi r_{s,i}^3 \right) \frac{(\rho_{s,i} - \rho_f)}{Q r_{s,i}} \left(\frac{\sin(Q r_{s,i})}{(Q r_{s,i})^2} - \frac{\cos(Q r_{s,i})}{Q r_{s,i}} \right) \right]^2. \quad (\text{F1})$$

The polydispersity of shell radius R_s of particle i is assumed to be

$$f(r_{s,i}) = \frac{1}{\sqrt{2\pi\sigma_{r_{s,i}}^2}} \exp\left[-\frac{(r_{s,i} - \langle r_{s,i} \rangle)^2}{2\sigma_{r_{s,i}}^2}\right]. \quad (\text{F2})$$

$\langle R_{s,i} \rangle$ and $\sigma_{R_{s,i}}$ are the average shell radius and standard deviation of shell radius of particle type i , respectively. The ensemble form factor of particle type i is

$$\langle P_i(Q) \rangle = \int P_i(Q) f(r_{s,i}) dr_{s,i}. \quad (\text{F3})$$

TABLE IV. Information for sample 2. Four kinds of core-shell particles with different shell scattering length densities (SLDs) and hollow cores are used for simulating heterogeneous compact domains with inaccessible pores. R_c , $\langle R_s \rangle$, σ_{R_s} , ρ_s , φ_p , and n are core radius, average shell radius, polydispersity of shell radius, SLD of the shell, volume fraction, and number density of each kind of particle, respectively.

Parameters	Particle 1	Particle 2	Particle 3	Particle 4
r_c (Å)	600	800	500	400
$\langle r_s \rangle$ (Å)	1200	1000	1000	900
σ_{r_s} (Å)	120	100	100	90
ρ_s (10^{14} m^{-2})	7.44	6.30	1.00	0.40
φ_p	0.002	0.005	0.003	0.004
n (10^{15} m^{-3})	276.31	1193.66	716.20	1309.92

TABLE V. Exact values and experimental values of accessible specific surface area $\frac{S_A}{V}$, accessible-surface-averaged scattering length density (SLD) ρ_A , and surface-averaged second moment parameter ρ_{2M}^2 , and heterogeneity parameter Δ_H^2 for sample 1 and sample 2. The exact structural parameters are directly calculated from the heterogeneous simulation system with known parameters described in Tables III and IV. The experiment parameters are extracted from GPSLM data analysis of simulated small-angle neutron scattering (SANS) intensity in Fig. 3.

Parameters	Sample 1	Sample 1	Sample 2	Sample 2
	Exact	GPSLM (Simulation)	Exact	GPSLM (Simulation)
$\frac{S_A}{V}$ (m^{-1})	128261	141087 ± 209	427536	456784 ± 619
ρ_A (10^{14}m^{-2})	3.4496	3.4487 ± 0.0006	3.4496	3.6317 ± 0.0006
ρ_{2M}^2 (10^{28}m^{-4})	31.56	30.73 ± 0.02	31.56	34.21 ± 0.02
Δ_H^2	0.6230	0.6129 ± 0.0002	0.6230	0.6144 ± 0.0001

The small-angle scattering intensity of this system can be calculated as

$$I(Q, \rho_f) = \sum_i [n_i \langle P_i(Q) \rangle], \quad (\text{F4})$$

where n_p is the number density of the particle p .

One example is given in the main text. We have also simulated the scattering patterns with similar surface heterogeneity, but with much smaller particle sizes. The simulated patterns are shown in Fig. 3. Figures 3(a) and 3(c) are for sample 1 with the sample information listed in Table III. And Figs. 3(b) and 3(d) are for sample 2 with the sample information listed in Table IV. Note that the curves in Figs. 3(c) and 3(d) are obtained by fitting 161 simulated SANS patterns by systematically varying ρ_f from 0 to $8 \times 10^{-6} \text{cm}^{-1}$. Table V lists the results obtained with the GPSLM compared with the exact values. Note that the error bars estimated in Table V are based on the assumption that any deviation from the theoretical values using the GPSLM is due to the statistics errors following the Gaussian distribution. This is just a guide to estimate theoretically how close the values from the GPSLM are to the exact values.

APPENDIX G: POROD'S SCATTERING DECOUPLED FROM OTHER SCATTERING FEATURES INDEPENDENT OF CONTRAST VARIATION

For scattering intensity that has both contributions from Porod's scattering and another scattering pattern, such as power-law decay, the GPSLM for the five cases being discussed may still be applicable if Porod's scattering can be decoupled and the rest of the scattering features do not depend on the SLD of the guest fluid. Here we derive the equations for the special case with scattering intensity formulated as Eq. (47). In this situation, we use a modified intensity ratio, $R_m(\rho_f) = \frac{I(Q, \rho_f) - I(Q, \rho_f = \rho_{f, \min})}{I(Q, \rho_f = 0) - I(Q, \rho_f = \rho_{f, \min})}$ [Eq. (47)], instead of $R(\rho_f)$ [Eq. (4)] to apply GPSLM.

Combining Eqs. (4), (5), and (46), we can write $I(Q, \rho_f)$ as

$$I(Q, \rho_f) = R(\rho_f) I_P(Q, \rho_f = 0) + C_f Q^{-a} = \left[\frac{1}{\rho_{2M}^2} (\rho_f - \rho_A)^2 + \Delta_H^2 \right] I_P(Q, \rho_f = 0) + C_f Q^{-a}. \quad (\text{G1})$$

Plugging $I(Q, \rho_f)$ into the definition of $R_m(\rho_f)$, we can obtain Eq. (48),

$$R_m(\rho_f) = \frac{I(Q, \rho_f) - I(Q, \rho_f = \rho_{f, \min})}{I(Q, \rho_f = 0) - I(Q, \rho_f = \rho_{f, \min})} = \frac{\left[\frac{1}{\rho_{2M}^2} (\rho_f - \rho_A)^2 \right] I_P(Q, \rho_f = 0)}{\left[\frac{1}{\rho_{2M}^2} \rho_A^2 \right] I_P(Q, \rho_f = 0)} = \frac{(\rho_f - \rho_A)^2}{\rho_A^2}. \quad (\text{G2})$$

-
- [1] Y. Liu and J. Wilcox, *Environ. Sci. Technol.* **46**, 1940 (2012).
[2] P. Zarzycki, P. Szabelski, and R. Charnas, *J. Comput. Chem.* **26**, 1079 (2005).
[3] M. Penna, K. Ley, S. Maclaughlin, and I. Yarovsky, *Faraday Discuss.* **191**, 435 (2016).
[4] B. Charnas and R. Lebeda, *J. Chromatogr. A* **886**, 133 (2000).
[5] K. N. Alstadt, K. S. Katti, and D. R. Katti, *J. Nanomech. Micromech.* **6**, 04015003 (2016).
[6] W. Zhu, J. J. Hughes, N. Bicanic, and C. J. Pearce, *Mater. Char.* **58**, 1189 (2007).
[7] C. Liu, Y. Liu, S. Kerisit, and J. Zachara, *Rev. Mineral. Geochem.* **80**, 191 (2015).
[8] E. Fathi and I. Y. Akkutlu, *Transp. Porous Media* **80**, 281 (2009).
[9] E. Biddiss, D. Erickson, and D. Li, *Anal. Chem.* **76**, 3208 (2004).

- [10] D. Erickson and D. Li, *Langmuir* **18**, 8949 (2002).
- [11] L. Lapčák, M. Otyepka, E. Otyepková, B. Lapčáková, R. Gabriel, A. Gavenda, and B. Prudilová, *Curr. Opin. Colloid Interface Sci.* **24**, 64 (2016).
- [12] R. Huang, R. P. Carney, F. Stellacci, and B. L. T. Lau, *Nanoscale* **5**, 6928 (2013).
- [13] R. Huang, R. P. Carney, K. Ikuma, F. Stellacci, and B. L. T. Lau, *ACS Nano* **8**, 5402 (2014).
- [14] A. Pappacena, M. Boaro, L. Armelao, J. Llorca, A. Trovarelli, J. M. Pintado, S. Bernal, J. A. P. Omil, and J. J. Calvino, *Catal. Sci. Technol.* **6**, 399 (2016).
- [15] D. Y. Murzin, *Ind. Eng. Chem. Res.* **44**, 1688 (2005).
- [16] E. M. Zuyderhoff, C. M. Dekeyser, P. G. Rouxhet, and C. C. Dupont-Gillain, *J. Colloid Interface Sci.* **319**, 63 (2008).
- [17] S. Kelly, H. El-Sobky, C. Torres-Verdín, and M. T. Balhoff, *Adv. Water Resour.* **95**, 302 (2016).
- [18] G. Betz, G. K. Wehner, L. Toth, and A. Joshi, *J. Appl. Phys.* **45**, 5312 (1974).
- [19] R. L. Moore, G. L. Grobe, and J. A. Gardella, *J. Vac. Sci. Technol. A Vacuum, Surfaces, Film.* **9**, 1323 (1991).
- [20] A. Tolbert and A. J. Ragauskas, *Energy Sci. Eng.* **5**, 5 (2017).
- [21] G. Porod, *Kolloid-Zeitschrift* **125**, 51 (1952).
- [22] G. Porod, *Kolloid-Zeitschrift* **124**, 83 (1951).
- [23] R. P. Rambo and J. A. Tainer, *Biopolymers* **95**, 559 (2011).
- [24] E. W. Kaler and IUCr, *J. Appl. Crystallogr.* **21**, 729 (1988).
- [25] D. Stoeckel, D. Wallacher, G. A. Zickler, J. Perlich, U. Tallarek, and B. M. Smarsly, *Phys. Chem. Chem. Phys.* **16**, 6583 (2014).
- [26] W.-S. Chiang, D. Georgi, T. Yildirim, J.-H. Chen, and Y. Liu, *Nat. Commun.* **9**, 784 (2018).
- [27] Y. B. Melnichenko, L. He, R. Sakurovs, A. L. Kholodenko, T. Blach, M. Mastalerz, A. P. Radliński, G. Cheng, and D. F. R. Mildner, *Fuel* **91**, 200 (2012).
- [28] X. Gu, D. F. R. Mildner, D. R. Cole, G. Rother, R. Slingerland, and S. L. Brantley, *Energy Fuels* **30**, 4438 (2016).
- [29] K. S. W. Sing, D. H. Everett, R. A. W. Haul, L. Moscou, R. A. Pierotti, J. Rouquerol, T. Siemieniewska, K. S. W. Sing, D. H. Everett, R. A. W. Haul, L. Moscou, R. A. Pierotti, J. Rouquerol, and T. Siemieniewska, in *Handbook of Heterog. Catal.* (Wiley-VCH Verlag GmbH, Weinheim, 2008).
- [30] P. L. Hall, D. F. R. Mildner, and R. L. Borst, *J. Geophys. Res.* **91**, 2183 (1986).
- [31] T. Pernyeszi and I. Dékány, *Colloid Polym. Sci.* **281**, 73 (2003).
- [32] S. Ciccariello, J.-M. Schneider, B. Schönfeld, and G. Kostorz, *Europhys. Lett.* **50**, 601 (2000).
- [33] W.-S. Chiang, E. Fratini, P. Baglioni, J.-H. Chen, and Y. Liu, *Langmuir* **32**, 8849 (2016).
- [34] W.-S. Chiang, E. Fratini, P. Baglioni, D. Georgi, J. Chen, and Y. Liu, *J. Phys. Chem. C* **120**, 4354 (2016).
- [35] N. Muroyama, A. Yoshimura, Y. Kubota, K. Miyasaka, T. Ohsuna, R. Ryoo, P. I. Ravikovitch, A. V. Neimark, M. Takata, and O. Terasaki, *J. Phys. Chem. C* **112**, 10803 (2008).
- [36] K.-H. Liu, Y. Zhang, J.-J. Lee, C.-C. Chen, Y.-Q. Yeh, S.-H. Chen, and C.-Y. Mou, *J. Chem. Phys.* **139**, 064502 (2013).
- [37] A. Petzold, A. Juhl, J. Scholz, B. Ufer, G. Goerigk, M. Fröba, M. Ballauff, and S. Mascotto, *Langmuir* **32**, 2780 (2016).
- [38] M. Sharifi, R. Marschall, M. Wilhelm, D. Wallacher, and M. Wark, *Langmuir* **27**, 5516 (2011).
- [39] O. Spalla, S. Lyonnard, and F. Testard, *J. Appl. Crystallogr.* **36**, 338 (2003).
- [40] K.-H. Liu, Y. Zhang, U.-S. Jeng, and C.-Y. Mou, *J. Chem. Phys.* **143**, 094704 (2015).
- [41] E. A. Chavez Panduro, T. Beuvier, M. Fernández Martínez, L. Hassani, B. Calvignac, F. Boury, and A. Gibaud, *J. Appl. Crystallogr.* **45**, 881 (2012).
- [42] A. P. Radlinski, E. Z. Radlinska, M. Agamalian, G. D. Wignall, P. Lindner, and O. G. Randl, *J. Appl. Crystallogr.* **33**, 860 (2000).